

POLITECNICO DI TORINO

Aerospace Engineering Master Thesis



POLITECNICO  
DI TORINO

# Automatic Preliminary Assessment of the mechanical response of LPT stages

**Candidate:**

Davide Prino

student ID: 235982

**Academic supervisor:**

Ing. Christian Maria Firrone

**Internal supervisor:**

Ing. Marco Moletta

December 2018



*"To be able to fill leisure intelligently is the  
last product of civilization"*

- Bertrand Russell

To my friends



## Acknowledgements

During the last six months I had the opportunity to write my master thesis in cooperation with GE Avio Aero, allowing me to experience the practical side of engineering, learning hands-on the scientific basis in the world of aircraft turbines. For this I would like to thank Ing. Marco Moletta, who made this collaboration possible. Furthermore I give thanks to colleagues Ing. Paride Mesaglio Chittaro and Ing. Szwed Witold and to fellow students Simone Claudio Concas, Gianluca Mosiello, Eleonora Caponio and Riccardo Scarpulla for their help and support.

I would like to express my gratitude to Prof. Christian Maria Firrone who guided me through my thesis work.

A special thank to my family who supported me with love during all my years at university.



# Abstract

The aim of this thesis work is the development of a tool (PRIME) able to make quick assessments of the mechanical response of a *Low Pressure Turbine* stage of aeronautical engines. It places itself in the preliminary design loops, giving aeromechanical feedback during the aerodynamic design, thus leading to an optimization process which includes both disciplines. The usual iterations between aerodynamic and aeromechanical design are reduced, allowing for a time effective process and a reduction of possible misunderstanding between teams.

The tool receives as inputs aerodynamic data, from which it generates the 3D airfoil, then it completes the CAD adding consistent inner and outer elements. The geometry is handled in the *Unigraphics NX* environment. Afterwards a *Finite Elements* model is created in *Ansys Workbench*. Here two different analyses can be run: the static analysis and the pre-stressed modal analysis. The latter provides the inputs to perform a flutter analysis and to study the forced response.

The focus of this work is placed in the setup and validation of the FE models for the static analysis in *Ansys Workbench*. The results obtained with this software must be consistent with the ones obtained with *msc NASTRAN*, where the legacy of AvioAero is built. Furthermore an already existing tool for the forced response analysis has been automatized in order to fit in the PRIME process.





# Contents

<b>1</b>	<b>Introduction</b>	<b>1</b>
1.1	The GREAT 2020 Project . . . . .	1
1.2	Thesis Purpose . . . . .	3
<b>2</b>	<b>Airbreathing Engine</b>	<b>5</b>
2.1	The Main Turbine Engine Architectures . . . . .	6
2.1.1	Turbojet . . . . .	6
2.1.2	Turboprop . . . . .	7
2.1.3	Turboshaft . . . . .	8
2.1.4	Turbofan . . . . .	8
2.2	Low Pressure Turbines . . . . .	9
2.2.1	LPT blading . . . . .	10
2.2.2	Contra-Rotating Turbine . . . . .	11
<b>3</b>	<b>Rotordynamics</b>	<b>15</b>
3.1	Modal Analysis . . . . .	16
3.1.1	Mode Shapes . . . . .	17
3.1.2	Modal Families and FreND Diagram . . . . .	23
3.1.3	Modal Assurance Criterion . . . . .	26
3.1.4	Cyclic Symmetry in FE Analysis . . . . .	26
3.2	Exciting Forces . . . . .	30
3.2.1	Forward and Backward EO . . . . .	31
3.2.2	Campbell Diagram . . . . .	33
3.2.3	Resonance Conditions . . . . .	34
<b>4</b>	<b>LPT Design</b>	<b>37</b>
4.1	Aerodynamic Design . . . . .	38
4.2	Structural Design . . . . .	40
4.3	Aero-Mech Design . . . . .	42

---

4.3.1	PRIME Today . . . . .	44
4.3.2	PRIME in the Future . . . . .	45
<b>5</b>	<b>Static Analysis</b>	<b>47</b>
5.1	Loads Acting on the Blade . . . . .	47
5.1.1	Inertial Load . . . . .	48
5.1.2	Pressure Load . . . . .	48
5.1.3	Thermal load . . . . .	49
5.1.4	Pre-Twist . . . . .	50
5.2	Static Analysis in PRIME . . . . .	51
5.2.1	Ansys Elements Investigation . . . . .	53
5.2.2	Inertial Load in PRIME . . . . .	54
5.2.3	Pressure Load in PRIME . . . . .	55
5.2.4	Thermal Load in PRIME . . . . .	57
5.2.5	Pre-twist in PRIME . . . . .	59
5.2.6	Complete Load Case . . . . .	61
<b>6</b>	<b>Forced Response</b>	<b>63</b>
6.1	@Forced for PRIME . . . . .	64
6.2	Tool Process . . . . .	65
<b>7</b>	<b>Conclusions</b>	<b>69</b>
<b>A</b>	<b>PRIME Routines Overview</b>	<b>71</b>
A.1	DynBooster . . . . .	71
A.2	Wizard . . . . .	74
A.3	@Forced . . . . .	76
A.4	AutoFlutter . . . . .	76
	<b>Bibliography</b>	<b>78</b>

# List of Figures

1.1	Great 2020 main goals . . . . .	2
2.1	Propulsion device working scheme. Subscript (0) is for entering conditions, while (e) is for exhausted quantities. $V$ is the velocity, $\dot{m}$ the mass flow, $p$ the pressure and $A$ the area. [4] . . . . .	5
2.2	Turbojet architecture [8] . . . . .	6
2.3	Turboprop architecture [8] . . . . .	7
2.4	Turboshaft architecture [10] . . . . .	8
2.5	Turbofan architecture [8] . . . . .	9
2.6	Blade and vane parts . . . . .	11
2.7	Sketch of a contra-rotating turbine architecture [16] . . . . .	12
2.8	Comparison of the axial length of a traditional turbine and a contra-rotating turbine. Vanes are in blue, co-rotating blades in red and contra-rotating blades in fuchsia. . . . .	12
3.1	Sector of a bladed disk in cyclic symmetry [6] . . . . .	17
3.2	Examples of deflected shapes with nodal diameters and nodal circumferences [6] . . . . .	18
3.3	Schematic representation of standing and rotating waves [4] . . . . .	21
3.4	Deflected shapes of a mode with $ND = 2$ , they can be seen as the real and imaginary part of a complex eigenvector [6] . . . . .	23
3.5	Example of the most common mode shapes for a blade. From left to right: edgewise (EW), flapwise (FW), bending (F), torsion (T) [6] . .	24
3.6	Examples of first and second order bending mode . . . . .	24
3.7	Example of FRENDD diagram with the mode shapes classification [10] . . . . .	25
3.8	Fundamental sector of a bladed disk where the cyclic symmetry region is marked in red [3] . . . . .	29
3.9	A disk with 4 blades excited by an harmonic force [6] . . . . .	31

3.10	On the left a forward rotating force, on the right a backward rotating force with harmonic index $n = 3$ [6] . . . . .	32
3.11	Campbell Diagram . . . . .	33
3.12	Aliasing phenomenon [24] . . . . .	35
3.13	EO on a sector [24] . . . . .	36
4.1	LPT cross section [10] . . . . .	37
4.2	2D-sketch of the flowpath of a 6 stages LPT. The corner points are identified by the symbol (+). R stands for rotor and S for stator [4] .	38
4.3	Velocity triangles of a LPT stage. The speed in the steady reference system is $c$ , while $w$ represents the velocity in a coordinate system rotating with the rotor. In order to achieve the optimal flowpath, the air must be deflected in specific directions, thus determining the leading and trailing edges geometry. [10] . . . . .	39
4.4	Turbine blade showing twisted contour [4] . . . . .	40
4.5	Traditional design workflow for LPT stages [10] . . . . .	41
4.6	Aero-Mech design representation [10] . . . . .	42
4.7	PRIME process. The focus of this thesis is placed in the building of the blocks encircled in red . . . . .	44
5.1	In figure (a) the cross-section of a turbine blade is shown, where the action of the airflow is represented by red arrows. In figure (b) a sketch of the working principle of camber practice is displayed [4] . . . . .	48
5.2	Development of turbine blade cooling [19] . . . . .	50
5.3	Pre-twist effect on the blade . . . . .	50
5.4	Peanuts plot example . . . . .	51
5.5	Blade Only model with important surfaces for FE analysis enlightened [12] . . . . .	52
5.6	Loads analyzed for the cantilevered beam model. . . . .	53
5.7	Pressure mapping on the nodes of a plate using triangulation and distance based average methods. The plot on the left is the source map. . . . .	56
5.8	Pressure mapping on the elements of a plate using triangulation and distance based average methods. The plot on the left is the source map. . . . .	56
6.1	@Forced GUI . . . . .	64
6.2	@Forced process . . . . .	65

---

6.3	Grid alignment. The red point is used for axial alignment, while the green point for radial alignment . . . . .	66
6.4	FRF: frequency response function . . . . .	67
A.1	2D airfoil and the parameters that define it [12] . . . . .	72
A.2	DynBooster GUI for templates selection . . . . .	73
A.3	WB project automatically generated by the Wizard for a blade only model. In this case all the analyses have been requested (peanuts plots computation, static analysis and modal analysis) . . . . .	75
A.4	Aeroplots example [7] . . . . .	77



# List of Tables

5.1	Second order tetrahedral elements comparison between WB and NS. .	54
5.2	Directional displacements results for inertial load . . . . .	54
5.3	Max principal stress results for inertial load . . . . .	55
5.4	Directional displacements results for pressure load . . . . .	57
5.5	Max principal stress results for pressure load . . . . .	57
5.6	Directional displacements results for thermal load . . . . .	58
5.7	Max principal stress results for thermal load . . . . .	58
5.8	Peanuts results . . . . .	59
5.9	Directional displacements results for pre-twist . . . . .	60
5.10	Max principal stress results for pre-twist . . . . .	60
5.11	Directional displacements results for the complete case . . . . .	61
5.12	Max principal stress results for the complete case . . . . .	61
A.1	Analyses available in the WB wizard . . . . .	74





## Nomenclature

AF	Airfoil
BC	Boundary Coindition
BO	Blade only
CAD	Computer aided design
CFD	Computational Fluid Dynamics
DOF	Degree of freedom
EO	Engine Order
EW	Edgewise
F	Bending
FEA	Finite element analysis
FEM	Finite element model
FRF	Frequency response function
FW	Flapwise
GUI	Graphic User Interface
HCF	High cycle fatigue
HPT	High pressure turbine
IBPA	Inter Blade Phase Angle
IBV	Inner band vane
IGV	Inlet Guide Vanes
LPT	Low pressure turbine
MAC	Modal Assurance Criterion
ND	Nodal diameter
NS	MSC Nastran
NS	Nastran
OBV	Outer band vane
ODS	Operating Deflection Shape
PS	Pressure side
ROM	Reduced Ordel Modelling
SS	Suction side
T	Torsional
WB	ANSYS Workbench



# Chapter 1

## Introduction

### 1.1 The GREAT 2020 Project

This thesis work places itself in a bigger project: GREAT 2020 (Green Engine for Air Traffic), to which many aeronautical companies take part. Among them Avio Aero, leader company for the project. This work was conducted in collaboration with it.

The project was born in 2009 when the European Commission and ACARE (Advisory Council for Aviation Research and Innovation in Europe) set new goals, to be reached within ten years, in order to meet the requirements of the expanding aeronautical industry, offering higher quality standards and economical and environmental friendly solutions [17]. In Piedmont (Italy) the project is backed up by the *Comitato Distretto Aerospaziale Piemonte* and financially sustained by the region.

GREAT 2020 aims to reduce chemical and noise pollution generated by aircraft engines. Specifically the main goals are to halve CO<sub>2</sub> emissions, to reduce NO<sub>x</sub> emissions by 80% and to reduce noise by 10dB. These being very challenging objectives, a great research effort must be put in the development of new solutions for every components of the propulsive system. The present work will focus on the low pressure turbine preliminary design.

In addition to meet the technological challenges, GREAT 2020 has also more general purposes, such as the creation of a solid research structure on aeronautics in Piedmont, the improvement of industry, research centers and education centers in Piedmont and the promotion of the *Distretto Aerospaziale* in Europe.

The main actors who participate to the project are:

- Avio Aero, a *GE Aviation* business, leader in the design, manufacturing and maintenance of civil and military aeronautical components and systems. Its work concerns mechanical transmissions and low pressure turbines.

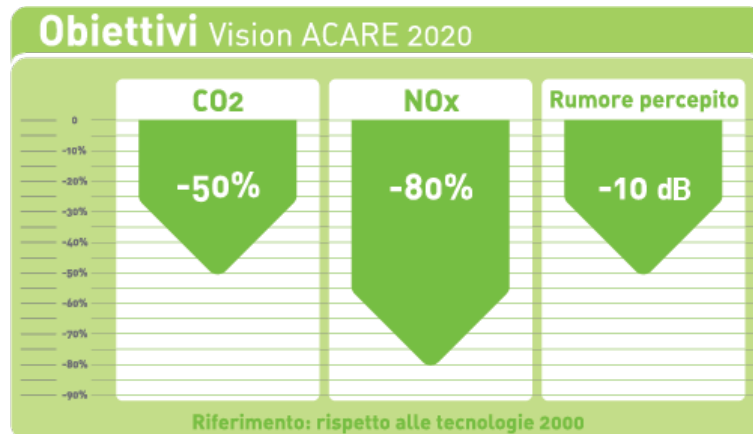


Figure 1.1: Great 2020 main goals

- Politecnico di Torino, one of the most prestigious public technical universities worldwide. The departments that give their contribution to the project are: the department of Mechanical and Aerospace Engineering, Applied Science and Technology, Energy and Management and Production Engineering.
- ISTEC-CNR, the Turin unit of Istituto di Scienza e Tecnologia dei Materiali Ceramici, which carries out research on ceramic materials. When it comes to the GREAT 2020 project, the institute helps in defining eco-friendly manufacturing processes for aeronautical alloys.

The project led to the birth of six laboratories, focusing on the development of strategic technologies useful in the manufacturing of the next generation of propulsive systems. They are all located in Piedmont and have a specific task:

- Lift Lab focuses on the development of low density and high resistance materials. It makes use of additive manufacturing to create turbine and burner components.
- Aeronflux Lab deals with the LPT optimization, in order to increase its efficiency and reduce the noise.
- Ageades Lab develops new robust technologies for the gearing of turbofan and open rotor engines.
- Zec Lab's task is to conceive the next generation of burners, which should be eco-friendly, safe and cheap.

- MC Lab focuses on the design of health monitoring systems for engines and devices for electric power generation, with an eye for the next 'more electric' engine generation.
- ECOPRO Lab has the goal to make the manufacturing processes environmental friendly.

## 1.2 Thesis Purpose

This thesis work concerns the preliminary design of low pressure turbines. It is part of a larger project carried out by Politecnico di Torino and GE Avio Aero. Its goal is to develop a tool (PRIME - Preliminary aeRoehysics Integrated Environment) able to automatically perform all needed mechanical and flutter analysis for the preliminary design of a LPT stage, starting from aerodynamic inputs. This will make possible the birth a new design concept: the Aero-Mech design. So far the design starts with aerodynamic studies, in order to find the optimal geometry that makes the conversion of energy from fluid to mechanical power as efficient as possible. Just after the airfoil is frozen, mechanical and flutter analyses are performed, to establish the resistance of the system to mechanical stresses and to assess the goodness of fluid/structure interactions. If the design fails one of the mandatory checks, it returns to the aero team, who has to modify the geometry consistently, then the cycle starts again. The PRIME tool allows a quick preliminary assessment of mechanic and aeroelasticity properties before the airfoil is frozen, including these discipline in the optimization loop and finding the best design which comply with multidisciplinary requirements.

The PRIME tool has to create the CAD, through a routine property of Avio Aero named DynBooster, then a finite element model (FEM) is created and the required analysis is run. The possible analyses are: static analysis and modal analysis. If the modal analysis was selected, the data to perform flutter analysis will be generated and the aeroelastic properties can be assessed, all information needed for the forced response are created too.

The focus of this work is on the static analysis and the forced response. Since the PRIME process must be automatic, in order to provide the user with a simple and fast tool, the finite element analysis (FEA) is run in ANSYS Workbench (WB) environment, because it is equipped with a solid and simple way to write wizards. Nevertheless all Avio Aero legacy is built on MSC Nastran (NS), so the new WB procedure must be validated against verified NS results.

Eventually, in order to preserve the intellectual property of the company, the results and graphics will be presented in a qualitative way and the parts will be referred to without specifying any absolute number of engine.

## Chapter 2

# Airbreathing Engine

The most common engine used in civil aviation is the airbreathing engine. It is a reaction engine, i.e. it makes use of Newton's third law of motion, which states: "for every force acting on a body there is an opposite and equal reaction". More specifically it is a esoreactor, indeed the working fluid used to propel the aircraft is air taken from the atmosphere, outside the engine. Ultimately, the working principle is to accelerate a certain mass of air backward in order to obtain thrust as a reaction. As the Newton's second law of motion states, the force is equal to the momentum flux, so the same amount of thrust can be generated either giving a large mass of air a little extra velocity or a small mass of air a large extra velocity [19], the former method being the more efficient one.

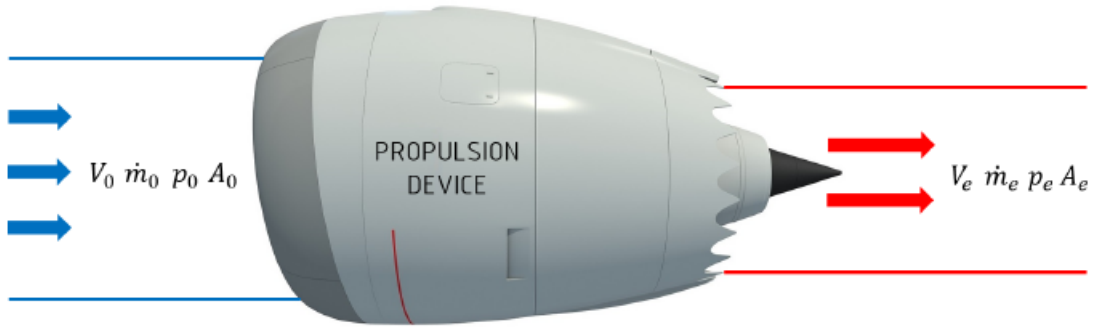


Figure 2.1: Propulsion device working scheme. Subscript (0) is for entering conditions, while (e) is for exhausted quantities.  $V$  is the velocity,  $\dot{m}$  the mass flow,  $p$  the pressure and  $A$  the area. [4]

Since aviation was still in its early stage, engineers were already thinking of using engines of this kind. In 1913 the french engineer Rene' Lorin patented a jet propulsion engine. It was similar to the modern ram jet, no turbomachines were used, all

compression and expansion of air occurs respectively in the intake and nozzle, resulting in very low efficiency at low speeds. Moreover at the time it was impossible to manufacture since high temperature resisting materials were not yet available. Some years later, in the 30s, Frank Whittle in England and Hans von Ohain in Germany, independently from one another, managed to build and run the first jet engines. With respect to the piston engine, the airbreathing engine has a much larger thrust per unit mass and per unit cross-sectional area and, since mass and size have always been critical issues when it comes to aircraft, it is no surprise that the turbo-engine became the principal propulsion technology in civil aviation.

## 2.1 The Main Turbine Engine Architectures

Even though the first turbine engines were turbojets, the outstanding advantages of this technology led to the birth of other configurations: turboprop, turboshaft and turbofan. In the following sections a brief description of each architecture is given.

### 2.1.1 Turbojet

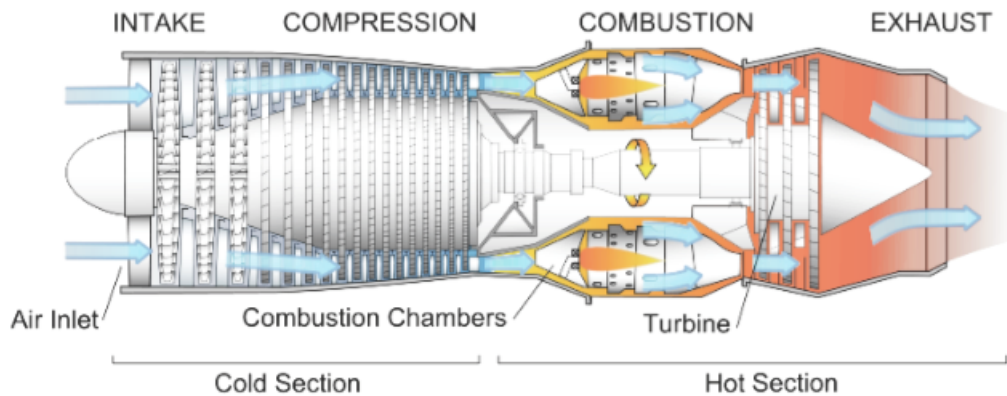


Figure 2.2: Turbojet architecture [8]

The turbojet was the most used configuration in the past and it paved the way for all new architectures available now. Its success is due to its high performance. Its introduction made possible the supersonic flight and greatly contributed to the costs reduction of air travel and the improvement in aircraft safety [13]. The air flows through the intake, which speeds down the flow and carries it to the compressor inlet, this way the compressor blades won't experience negative transonic effects when the



aircraft is flying at high speed. After the air is compressed, it is heated in the burner, where it is mixed with fuel and burned. Eventually the expansion is carried out in the turbine, that absorbs just enough power to drive the compressor, and in the nozzle, where the flow reaches high speed and is finally ejected.

### 2.1.2 Turboprop

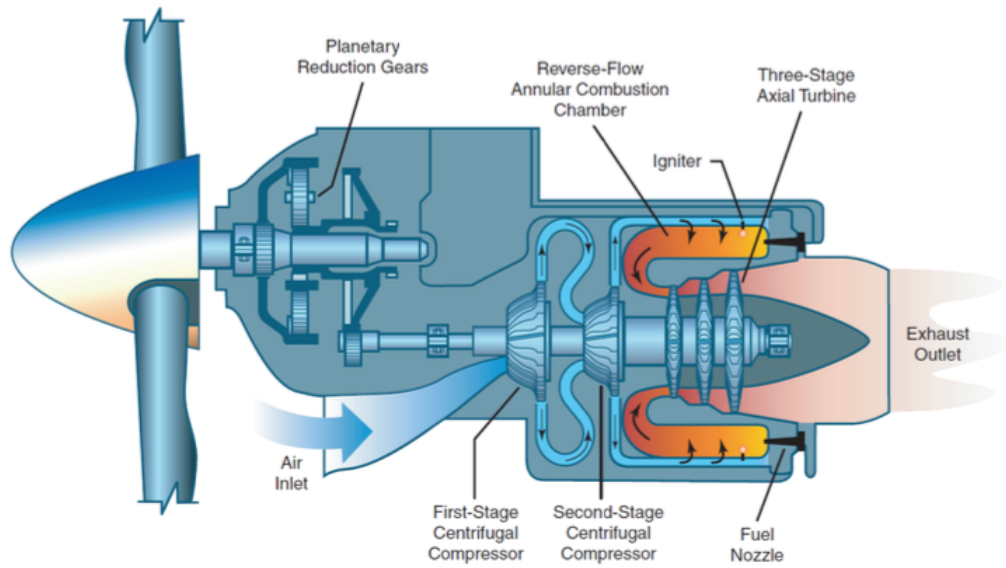


Figure 2.3: Turboprop architecture [8]

The core of the turboprop engine is similar to the turbojet engine, it consists of intake, compressor, burner, turbine and exhaust. Nevertheless the thrust is provided in two different ways: while the turbojet accelerates a relatively small mass of air through a nozzle, the turboprop engine makes use of a propeller to move a large mass of air backward, thus obtaining high propulsive efficiency. The principal drawback of this system is the flow speed limit on the propeller, indeed a large relative velocity leads to transonic effects lowering its efficiency. Moreover the rotational speed of the propeller shall be limited, because it requires a complex and heavy gearbox to join the high velocity power shaft with the low velocity propeller shaft. A more diffused way of solving this problem is to mount the compressor and the propeller on two different shafts, so that they can rotate independently from one another, implementing the multi-shafts turboprop configuration. A small turbine provides the compressor with the power it needs, but the largest amount of work is done on the power turbine,

which drives the propeller. This architecture is most suitable for relatively slow aircraft, where low fuel consumption is the major requirement.

### 2.1.3 Turboshaft

The turboshaft configuration is identical to the turboprop architecture, with the exception that the propeller is mounted transversely with respect to the engine axis. In this case it is not the engine that have to withstand the loads generated by the propeller, but is the gearbox, which is mounted on the aircraft structure [12]. This solution is mostly used in helicopters.

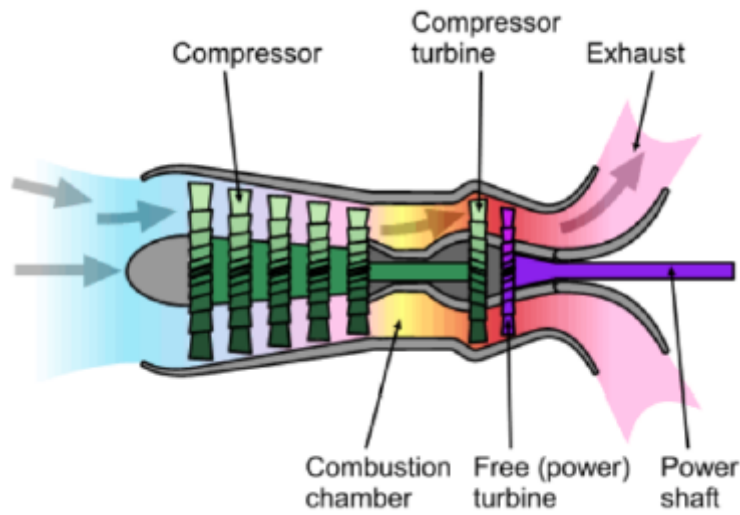


Figure 2.4: Turboshaft architecture [10]

### 2.1.4 Turbofan

The turbofan configuration is a compromise between turbojet and turboprop. It introduces a fan upstream the compressor, it behaves in a similar way to the propeller, but, since the fan is mounted inside a duct, the air flow can be controlled by the intake, allowing the aircraft speed to rise without incurring in undesired transonic effects and efficiency losses. The fan compresses a large amount of air, then the flow is split in two. The larger flow rate by-passes the hot core of the engine, i.e. where the burner is, while a small part of it is further compressed, heated and then expanded in two turbines. One of these turbines, the high pressure turbine (HPT), drives the compressor, while the other, the low pressure turbine (LPT), drives the fan and, in

some cases, the first compressor stages as well. Eventually the hot gases are ejected through a nozzle. This configuration introduces a new design parameter with respect to the traditional ones (compression pressure ratio and turbine inlet temperature) which is the by-pass ratio, i.e. the ratio between cold and hot air flow. Aircraft used in civil aviation have usually high by-pass ratio (6:1), while for supersonic flight a low by-pass ratio is required and the hot and cold fluxes are mixed before being expelled. To sum up, the advantage of these engines is the fact that they deal with a larger airflow with smaller speed with respect to the turbojet engines, thus having a larger propulsive efficiency, but they can still withstand larger flight speeds w.t.r. turboprop engines. Choosing the by-pass ratio is a trade off that can be made between fuel consumption and performance of the aircraft.

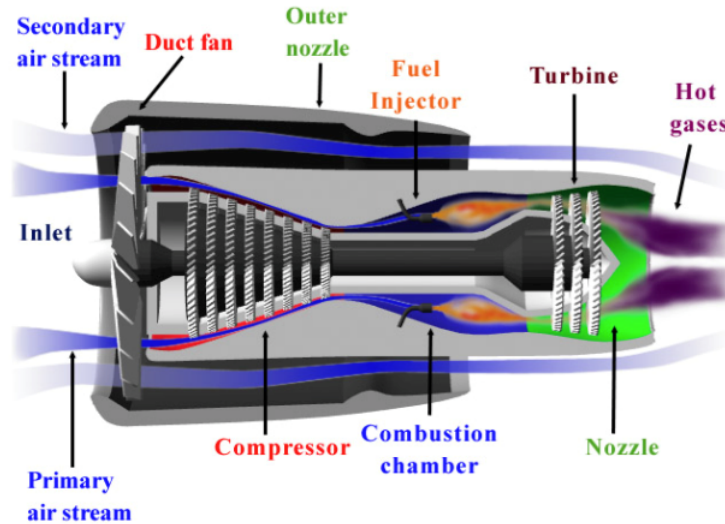


Figure 2.5: Turbofan architecture [8]

## 2.2 Low Pressure Turbines

Since the present work concerns the preliminary design of LPT stages of airbreathing engines, these components are explained further in this section. This thesis was carried out on parts designed and manufactured by Avio Aero and mounted on GE Aviation engines. As aforementioned, the low pressure turbine drives the fan and some compressor stages. It extracts energy from the hot gases and converts it into mechanical power on a shaft. Since airbreathing engines need to process a very large airflow, axial turbomachines are preferred over their radial counterparts, even though

the pressure ratio attainable with a single stage of an axial turbine is low. However this problem can be easily overcome using multistage turbines.

The design of LPT stages has some criticalities on account of the harsh environment they have to cope with. First of all the gases coming from the burner are very hot and, since the turbine inlet temperature should be as high as possible in order to rise both thermal efficiency and thrust per unit rate of airflow through the core engine, the trend is to further increase this temperature. The threshold is set by the ability of the turbine parts to withstand creep, challenging the designers to find new methods for cooling these parts and new materials able to withstand high temperatures under large loads. The design process also takes into account the turbine efficiency. The principal losses which lead to an overall efficiency of approximately 92% are aerodynamic losses and gas leakages.

### 2.2.1 LPT blading

The LPT stage is made of two parts: the stator and the rotor. The former is a row of stationary vanes, their task is to direct the flow toward the rotor blades and to accelerate it, by reducing its pressure. The rotor is made of blades mounted on a disk, here the power is transferred from the fluid to the shaft. The pressure acting on the blades makes them rotate, this rotation is transferred to the shaft by the disk. Vanes and blades interact with the flow and have an airfoil shape, defined, in first approximation, by the velocity triangles, on the basis of the desired expansion ratio in order to attain the needed performance.

If the pressure drop occurs only in the vane row, the turbine stage is called impulse stage. On the contrary, if the stator is designed only to divert the flow without changing its pressure, the stage is of the reaction type. Usually turbine stages are a combination of the two, the degree of reaction is defined as the fraction of the enthalpy drop occurring in the rotor and the overall drop of the stage.

The vane can be assumed as a beam fully constrained at its ends. The joints are made with two elements attached to the airfoil: the outer band vane (OBV) and the inner band vane (IBV). The vane has to withstand bending loads applied by the gases, as well as thermal loads, nevertheless heat resistance is the principal property required.

When it comes to blade constraints, its hub is jointed to the disk, while its tip is in interlocking with the adjacent blades. The contact between blade and disk is made through the dovetail, which is mounted under the shank, in charge of sustaining the airfoil. At the tip there is the shroud, which has two main tasks: to damp the

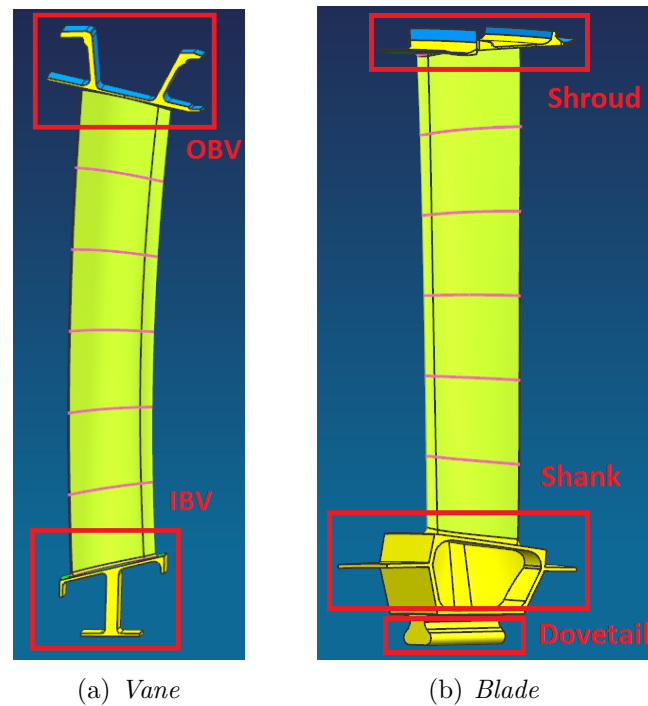


Figure 2.6: Blade and vane parts

oscillations through sliding contact with neighboring blades and to reduce leakages due to the gap existing between the blade tips and the casing, which provides the blade room to expand. In addition to the loads the vane has to cope with, the blade has to deal with centrifugal forces.

The airfoil of both vane and blade is twisted in order to have the same work along the radial direction and to ensure that the flow entering the exhaust system has uniform axial velocity [19]. Blades can also be hollow to let a flow of cooling air pass through them.

### 2.2.2 Contra-Rotating Turbine

In order to comply with rising requirements for aircraft engine efficiency and fuel consumption level, considering the restrictions in weight and size airborne systems are subjected to, new designs for all engine components should be considered. The contra-rotating turbine is one possible way to improve the turbine characteristics. The most common configuration has one row of static vanes at the turbine intake, which guides the flow toward a series of blade rows. These are attached to two shafts rotating in opposite directions, as shown in figure 2.7.

The main advantages of this design are [15]:

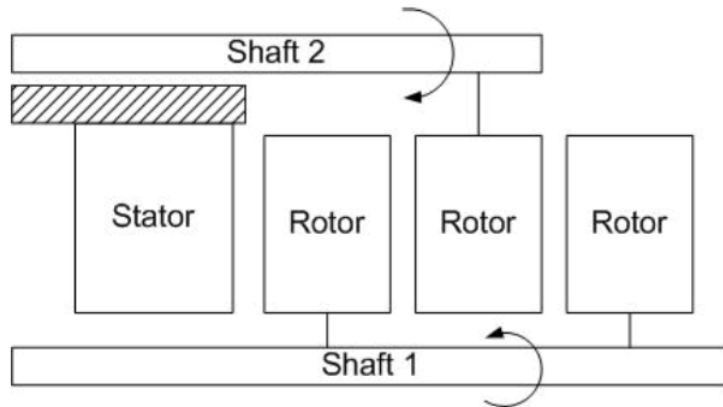


Figure 2.7: Sketch of a contra-rotating turbine architecture [16]

- increment of work per unit mass flow, due to large changes in angular momentum made possible by large relative velocities
- reduction of weight and axial length, due to the elimination of the vane rows. A study conducted in 2009 [16] demonstrated that using a counter-rotating turbine with the same number of stages as a traditional turbine (see figure 2.8) leads to the same performance level, decreasing length and weight.
- rising in efficiency, since it eliminates leakages and cooling losses associated with vanes.

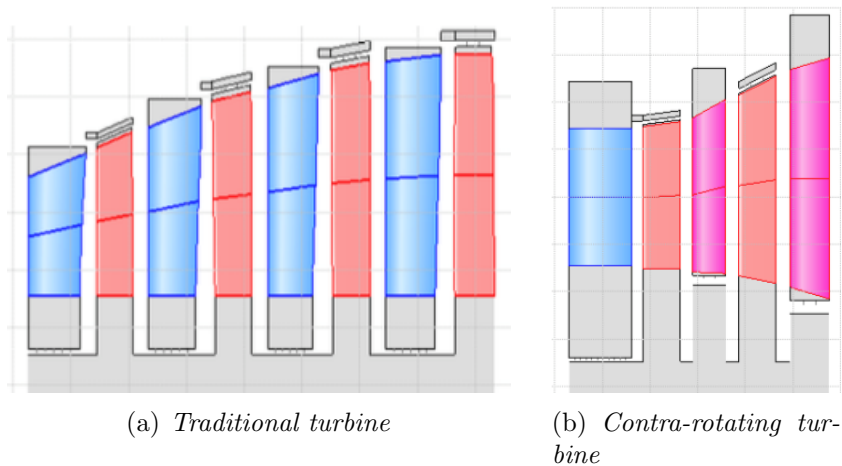


Figure 2.8: Comparison of the axial length of a traditional turbine and a contra-rotating turbine. Vanes are in blue, co-rotating blades in red and contra-rotating blades in fuchsia.

Since the aircraft engines work in off-design conditions for a large part of their life,

off-design performances are of the greatest importance. The contra-rotating turbine scores high in these conditions too with respect to the traditional one.

The principal drawback of this design is the great complexity of the flow path. Lately many steps forward have been made in the aerodynamic analysis of these phenomena, making the future development of compressors and fans using the contra-rotating architecture possible, reducing weight and size of aeronautical engines even more. Nevertheless the study of this technology is still in its early stage. This thesis work places itself in this scenario, since it aims to develop a tool for fast and automatic preliminary design analysis, very useful when trying to study the benefits of many possible configurations.





## Chapter 3

# Rotordynamics

Vibrations in gas turbines are known to be the principal cause of component failure. Due to the geometry of the rotor stage and its rotational velocity, the dynamic loads acting on the bladed disk show a periodical behavior. This can induce resonance phenomena, which will eventually lead the structure to exceed its fatigue limits, causing the rupture of the component. Turbine blades are particularly susceptible to high cycle fatigue damage due to the large range in frequency responses excited by the rotation, indeed each throttle setting means a different rotational speed and different cyclic and steady stresses induced by thermal and mechanical loads [25]. Hence dynamic analysis is of fundamental importance in the design of reliable turbomachines, since it predicts the oscillations frequencies under resonance conditions, these frequencies must lay outside the operative range of the engine.

There are two main sources of vibrations, studied by two different types of dynamic investigations:

- The *forced response* deals with the perturbations in the air flow generated by the upstream and downstream stages. These disturbances act as an exciting force on the rotor, which encounters them during its motion. Since the spacing between each couple of airfoils on the disk is even, the exciting action has an harmonic behavior. The frequency of the exciting action depends upon the rotational velocity of the shaft and the number of blades of adjacent stages.
- *Flutter analysis* is part of the dynamic aeroelasticity branch, which studies the interaction between fluid and structure and involves three disciplines: aerodynamics, elasticity and dynamics. Flutter instability is an auto-excited oscillation, where the elastic motion of the structure generates the aerodynamic forces needed to sustain or even magnify itself.

### 3.1 Modal Analysis

In engineering practice, vibrations characteristics are determined by natural frequencies and corresponding mode shapes. Modes are inherent properties of a structure, they are determined by material properties (mass, stiffness and damping properties) and boundary conditions of the structure. In the early days of turbines design, the blades were assumed as single beams cantilevered at their root. Then it was showed that the inclusion of shroud and disk in the analysis leads to the prediction of many more natural frequencies and modes, since all the blades behave as a system and are coupled through these components [21]. Nowadays a *modal analysis* is performed on a FE (Finite Element) model of the bladed disk, in order to obtain the natural frequencies and mode shapes, which will then be used in the forced response and flutter analysis.

In a FE analysis the geometry is divided into many small elements by a procedure called meshing, the finer the mesh the more accurate the results. A number of nodes is associated to each element, depending on the shape and the order of the element (i.e. the order of the function used to describe the solution over the element). All the nodes have an amount of degrees of freedom (DoFs) connected to them. This discretization is used to build the matrices which compose the equation of motion, typical of all structural problems.

$$[M]\{\ddot{x}(t)\} + [C]\{\dot{x}(t)\} + [K]\{x(t)\} = \{f(t)\} \quad (3.1)$$

where  $[M]$ ,  $[C]$  and  $[K]$  are respectively the mass, damping and stiffness matrices,  $\{x\}$  is the vector containing the DoFs (i.e. the three nodal directional displacements) and  $\{f\}$  is the vector of the external forces. If  $n_n$  is the number of nodes, the length of  $\{x\}$  and  $\{f\}$  is  $3n_n$  and the matrices are square matrices with dimension  $3n_n$ .

The modal analysis consists in finding the solution of the undamped system with no external excitation. So equation 3.1 is reduced to the following eigenproblem.

$$([K] - \omega_i^2[M])\{u_i\} = \{0\} \quad i = 1, \dots, N \quad (3.2)$$

where  $\omega_i^2$  and  $\{u_i\}$  are the  $i^{th}$  eigenvalue and eigenvector respectively. The eigenvalues are the natural frequencies and the eigenvectors represent the deformed structure, thus the mode shapes. While a real structure has an infinite number of modes, in FE analysis the maximum number of eigenvalues is equal to the number of Dofs. Since the problem is homogeneous, the non trivial solution contains an unknown constant and the displacements computed by software like NASTRAN and Ansys Workbench

doesn't have any physical meaning. Just the shape of the deformed structure can be predicted.

In industrial practice, a *pre-stressed modal analysis* is usually performed. A FE static analysis is performed first under the applied loads, that may include: centrifugal forces, pressure loads due to the interaction with the fluid, a thermal load, since the gases coming from the burner are hot, and a pre-twist of the blade. Among all these loads, the predominant one is the inertial load. The displacement and stress solutions are then used as initial conditions for the modal analysis [14].

### 3.1.1 Mode Shapes

The bladed disk is a structure which have rotational periodicity or cyclic symmetry, this means that if the geometry for any radial and axial position is defined at some angle  $\theta$ , it is identical at  $(\theta + n\phi_0)$ , where  $\phi_0$  is  $2\pi/N$ ,  $N$  being the number of blades and  $n$  any integer less than  $N$ . It follows that, if the geometry has been defined over a sector, the reminder of the structure can be obtained by repeated rotation of the substructure. To make the concept more clear, the sketch of a bladed disk where a sector has been cut off is shown in figure 3.1. Some further insight on cyclic symmetry and how it is applied in FE analysis is given in chapter 2.1.4.

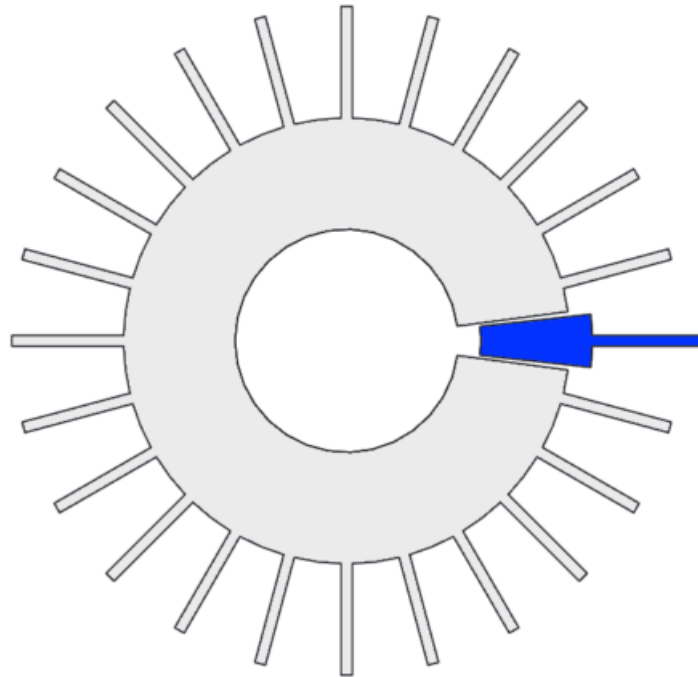
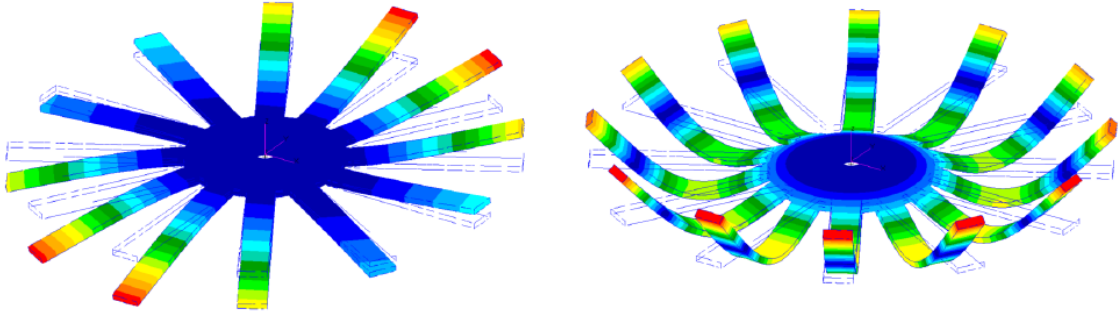


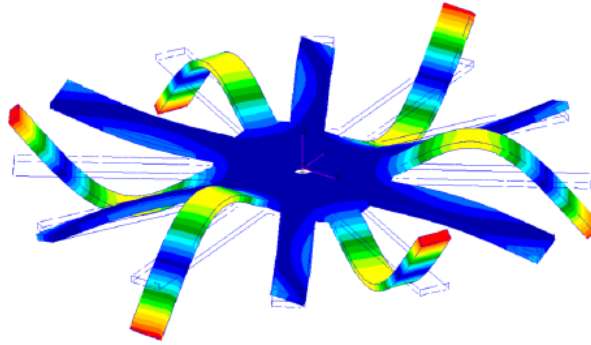
Figure 3.1: Sector of a bladed disk in cyclic symmetry [6]

The mode shapes of a structure with rotational periodicity present some typical features called *nodal diameters* (ND) and *nodal circumferences*. The former are straight lines passing through the disk center, where the modal displacement is null, similarly the latter are concentric circles with null modal displacement. Some examples of deflected shapes of a bladed disk with 12 sectors, which present these features are shown in figure 3.2.



(a) 1 nodal diameter and 0 nodal circumferences

(b) 0 nodal diameters and 1 nodal circumferences



(c) 3 nodal diameters and 1 nodal circumferences

Figure 3.2: Examples of deflected shapes with nodal diameters and nodal circumferences [6]

A thorough description of the mode shapes of a structure in cyclic symmetry is given in a paper by D. L. Thomas [23]. When solving the eigenproblem described by equation 3.2, it is convenient to rearrange the matrices and vectors such that the  $n_s$  Dofs of each sector are followed by the  $n_s$  Dofs of the next sector. This way an eigenvector of the whole structure can be written as

$$\{u\} = \{u^{(1)} \ u^{(2)} \ u^{(3)} \ \dots \ u^{(N)}\}^T \quad (3.3)$$

where  $\{u^{(i)}\}$  is a vector containing the displacements associated with the  $n_s$  degrees of freedom of the  $i^{th}$  substructure.

Rotationally periodic structures have a feature in common with axisymmetric geometries: most modes of vibration occur in degenerate orthogonal pairs. This is because, if a mode has a maximum deflection at some point of the structure, rotating the mode shape through an angle doesn't change the frequency of vibration. The modes can be classified into three classes, on the basis of the relationship between the shapes for individual sectors:

- (a) Each sector has the same mode shape as its neighbor.

$$\{u^i\} = \{u^{(i+1)}\} \quad \forall i \quad (3.4)$$

It doesn't show degeneracy, rotating the mode through any integer number of substructures leaves it unchanged, no other mode shape is needed to describe the rotation. The eigenvector can be written as follow:

$$\{u\} = \{u^{(1)} \ u^{(1)} \ u^{(1)} \ \dots \ u^{(1)}\}^T \quad (3.5)$$

- (b) Each sector has the same mode shape as its neighbor, but is vibrating in antiphase.

$$\{u^i\} = -\{u^{(i+1)}\} \quad \forall i \quad (3.6)$$

It doesn't show degeneracy, a rotation of the mode through an even number of substructures leaves it unchanged, while a rotation through an odd number makes it become  $-u$ , which is not a new mode shape, but a change of phase of  $\pi$ . The eigenvector can be written as:

$$\{u\} = \{u^{(1)} \ -u^{(1)} \ u^{(1)} \ \dots \ u^{(1)} \ -u^{(1)}\}^T \quad (3.7)$$

- (c) All other mode shapes show degeneracy, an orthogonal pair of eigenvectors must be used to describe the rotation of the mode shape.

$$\{u^i\} \neq \{u^{(i+1)}\} \quad \{u^i\} \neq -\{u^{(i+1)}\} \quad \forall i \quad (3.8)$$

For class (c) eigenvectors some further considerations are needed. The deflected shape  $\{u'\}$  obtained by rotating  $\{u\}$  round one sector, is also an eigenvector, distinguishable from  $\{u\}$  and not orthogonal to it in general.  $\{u'\}$  has the form:

$$\{u'\} = \{u^{(N)} \ u^{(1)} \ u^{(2)} \ \dots \ u^{(N-1)}\}^T \quad (3.9)$$

To allow the existence of  $\{u'\}$  there must be an eigenvector  $\{\bar{u}\}$  orthogonal to  $\{u\}$ , the two together make the basis of a vectorial space. All real solutions of the eigenproblem

are part of this vectorial space. Thus  $\{u'\}$  can be expressed as a linear combination of the two orthogonal vectors.

$$\{u'\} = c\{u\} + s\{\bar{u}\} \quad (3.10)$$

where  $c$  and  $s$  are constants. The orthogonal vector to  $\{u'\}$  can also be written as a linear combination of  $\{u\}$  and  $\{\bar{u}\}$

$$\{\bar{u}'\} = -s\{u\} + c\{\bar{u}\} \quad (3.11)$$

Thus the vectors  $\{u'\}$  and  $\{\bar{u}'\}$  can be expressed as a transformation of  $\{u\}$  and  $\{\bar{u}\}$

$$\begin{Bmatrix} u' \\ \bar{u}' \end{Bmatrix} = \begin{bmatrix} cI_{Nn_s} & sI_{Nn_s} \\ -sI_{Nn_s} & cI_{Nn_s} \end{bmatrix} \begin{Bmatrix} u \\ \bar{u} \end{Bmatrix} = [R] \begin{Bmatrix} u \\ \bar{u} \end{Bmatrix} \quad (3.12)$$

where  $I_{Nn_s}$  is the unit matrix of order  $N \cdot n_s$ . Clearly,  $[R]^i$  is a transformation matrix which rotates the mode shape round  $i$  sectors. Assuming the eigenvectors to be normalized such that  $\{u\}^T \{u\} = 1$ , the constants  $c$  and  $s$  can be expressed as  $\cos(\psi)$  and  $-\sin(\psi)$  respectively.  $\psi$  is the angle of which  $\{u\}$  must be rotated to obtain  $\{u'\}$ , it is called *Inter Blade Phase Angle* (IBPA), it describes the phase difference in the modal displacement between two neighboring blades and is described by the following equation:

$$\psi = \pm \frac{2\pi}{N} ND \quad (3.13)$$

where  $ND$  is the *Nodal Diameter*, a measure of the periodicity of the mode shape over the structure.

According to equations 3.10 and 3.11, any linear combination of  $\{u\}$  and  $\{\bar{u}\}$  is a solution of equation 3.2 with the same eigenvalue, also the complex vector  $\{z\}$  satisfies equation 3.2.

$$\{z\} = \{u\} + i\{\bar{u}\} \quad (3.14)$$

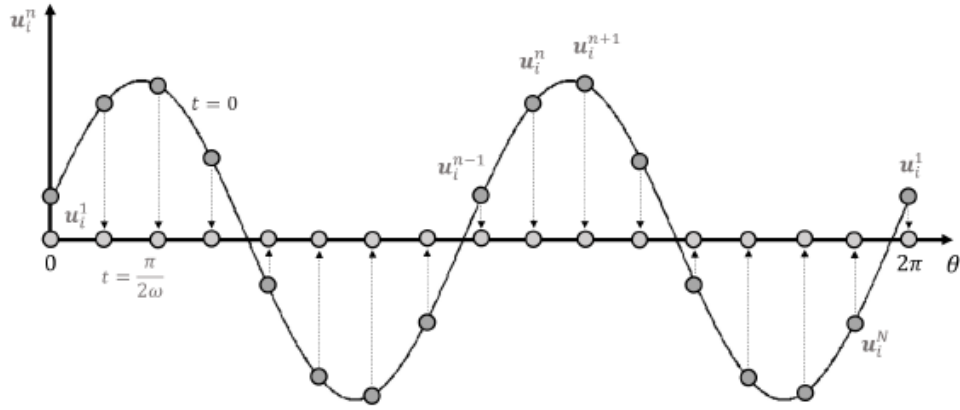
The complex vector contains the definition of both  $\{u\}$  and  $\{\bar{u}\}$ . Considering this definition, equation 3.12 can be rewritten as

$$\{z'\} = e^{-i\psi} \{z\} \quad (3.15)$$

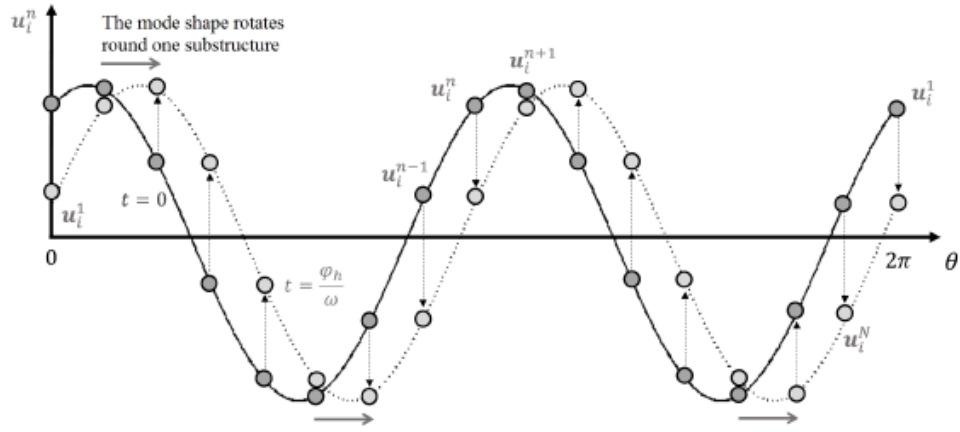
The deflections of any substructure can be written in terms of the deflections of any other

$$\{z^{(i-1)}\} = e^{-i\psi} \{z^i\} \quad (3.16)$$

The physical meaning of real and complex eigenvectors is related to their time evolution over the cyclic symmetric structure. The real eigenvectors of cases (a) and



(a) Standing wave, the peaks don't change position



(b) Rotating mode, the position of the peaks shifts in time

Figure 3.3: Schematic representation of standing and rotating waves [4]

(b) denote standing wave mode shapes, where the peaks of the deflected shape always occur at the same points. The mode shape of the structure at a given time is  $\{u\}e^{i\omega t}$ , where the real part of this complex quantity, i.e.  $\{u\}\cos(\omega t)$ , is the instantaneous deflected shape. Instead the complex vector  $\{z\}$  represents a rotating mode, in which the same instantaneous deflected shape reappears after successive time intervals  $t = \psi/\omega$ . The real part of  $\{z\}e^{i\omega t}$  gives the instantaneous deflected shape. If  $\{z\}$  is a clockwise rotating mode, there is another linear combination of  $\{u\}$  and  $\{\bar{u}\}$ , which gives a counterclockwise rotating mode  $\{\bar{z}\} = \{u\} - i\{\bar{u}\}$ .

For a better understanding of standing wave and rotating mode shapes, in figure 3.3 are displayed two schematic representations of the two different mode shapes. Regardless of the class, the instantaneous modal shapes can always be described as a combination of harmonic functions  $\cos(n\theta)$  or  $\sin(n\theta)$ ,  $\theta$  is the circumferential

coordinate and  $n$  (or ND) is the nodal diameter number. The maximum number of nodal diameters is function of the number of blades ( $N$ ):

$$\begin{cases} 0 \leq n \leq \frac{N}{2}, & \text{if } N \text{ is even} \\ 0 \leq n \leq \frac{N-1}{2}, & \text{if } N \text{ is odd} \end{cases} \quad (3.17)$$

Given a turbine stage with a definite number of blades, the *Inter Blade Phase Angle* can be used to delineate the periodicity of the mode of vibration, as well as ND. Even though ND is an integer, the IBPA can assume negative values. If positive values correspond to clockwise rotating mode shapes, negative values will be associated to counterclockwise rotating modes. The values that  $\psi$  can assume are:

$$\psi \in \left[ -\pi, -\frac{2\pi(N/2-1)}{N}, \dots, -\frac{4\pi}{N}, -\frac{2\pi}{N}, 0, \frac{2\pi}{N}, \frac{4\pi}{N}, \dots, \frac{2\pi(N/2-1)}{N}, \pi \right] \quad (3.18)$$

if  $N$  is even and:

$$\psi \in \left[ -\frac{2\pi(N-1)}{N}, \dots, -\frac{4\pi}{N}, -\frac{2\pi}{N}, 0, \frac{2\pi}{N}, \frac{4\pi}{N}, \dots, \frac{2\pi(N-1)}{N} \right] \quad (3.19)$$

if  $N$  is odd.

Finally the definitions of the classes of modes can be completed associating them to the corresponding values of  $\psi$  and ND:

- Class (a) modes can be represented as a standing wave over the circumference of the bladed disk, all the sectors are vibrating in-phase with each other. Thus both IBPA and ND are equal to 0. The mode is characterized by a single real eigenvector ( $e^{i\psi} = 1$ ). It exists for every rotationally periodic structure.
- Class (b) modes can also be represented by a standing wave and are characterized by a single real eigenvector ( $e^{i\psi} = -1$ ), but the substructures are vibrating in anti-phase. This condition can be met only if the disk has an even number of blades, since to have  $\psi = \pm\pi$ , the nodal diameter must be  $N/2$ .
- Class (c) modes are rotating modes and are characterized by complex eigenvectors. Each substructure has a phase difference of  $\psi$  with respect to its adjacent sectors. The nodal diameter comply with the following requirements:

$$\begin{cases} 0 < ND < \frac{N}{2}, & \text{if } N \text{ is even} \\ 0 < ND \leq \frac{N-1}{2}, & \text{if } N \text{ is odd} \end{cases} \quad (3.20)$$

An example of a rotating mode is given in figure 3.4.



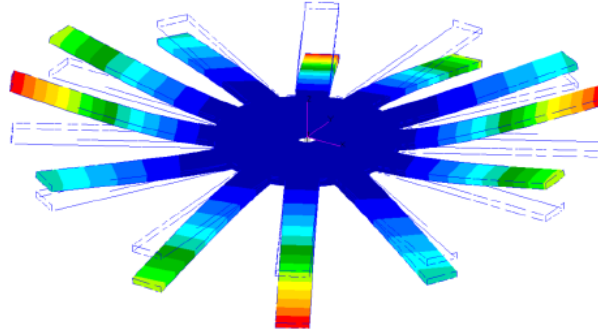
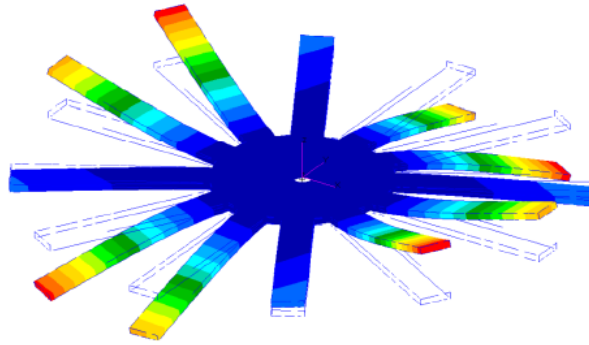
(a) *First deflected shape*(b) *Second deflected shape*

Figure 3.4: Deflected shapes of a mode with  $ND = 2$ , they can be seen as the real and imaginary part of a complex eigenvector [6]

### 3.1.2 Modal Families and FreND Diagram

Since the number of modes associated to a nodal diameter are equal to the number of degrees of freedom, for real continuous structures there is an infinite amount of natural frequencies and corresponding mode shapes. Instead for FE models, where the DoFs are limited by the number of elements the structure is divided into, the number of modes is finite, but still very large. Nevertheless, in engineering practice, only the first frequencies for each nodal diameter are taken into account.

Modes can be classified on the basis of the deflected shape. The most common ones that show themselves inside the range of frequencies usually considered are: edgewise (EW), flapwise (FW), bending (F), torsion (T). An example of this classification is shown in figure 3.5. From the bending mode on, the notation just seen is usually preceded by a number, which stands for the order of the mode shape. For instance 2F denotes a second order bending mode. The order can be seen as the number of peaks in the deflected shape. To clarify the concept, figure 3.6 displays a 1F and a 2F mode.

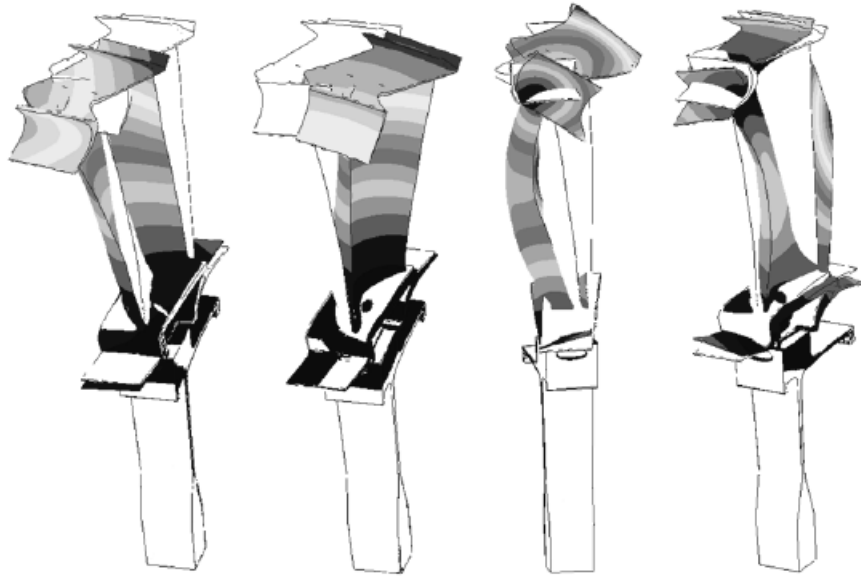


Figure 3.5: Example of the most common mode shapes for a blade. From left to right: edgewise (EW), flapwise (FW), bending (F), torsion (T) [6]

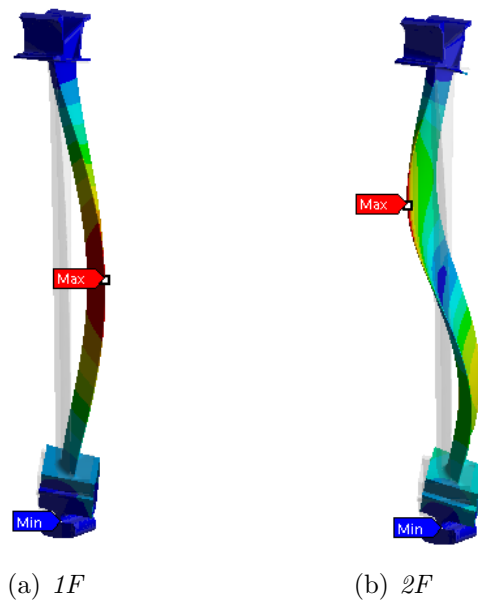


Figure 3.6: Examples of first and second order bending mode

Modes are usually grouped into *Modal Families*, just one natural frequency for each nodal diameter can be part of family. Two classification methods can be used to assort the modal families:

- on a frequency basis, e.g. the first family contains the smallest frequency for all the NDs, the second family all the second frequencies and so on;
- on a mode shape basis, e.g. each family is a group containing all the modes with identical deflected shape.

Modal Families are represented on the FREND (*FRE*quency - *Nodal Diameter*) diagram. On the x-axis is ND, while the frequency lays on the y-axis. Each line is a family, where the natural frequency is plotted against ND.

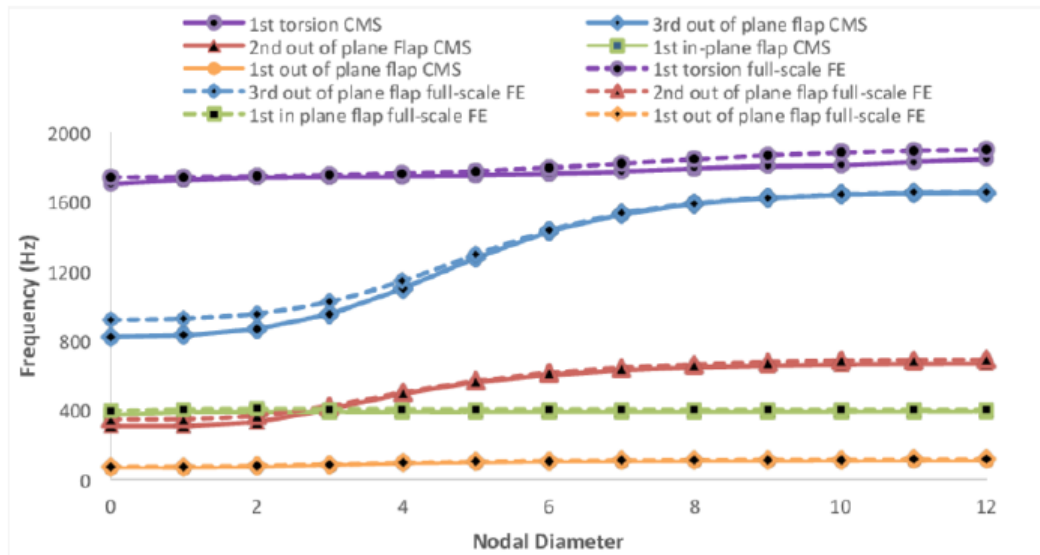


Figure 3.7: Example of FREND diagram with the mode shapes classification [10]

As it can be seen from figure 3.7, the curves for small ND values may have a growing behavior, then they approach to an asymptote. The diameters where the frequency grows represent modes of the disk, i.e. the blades are nearly undeformed, while the modes with larger ND values are modes of the blade, i.e. the disk behaves almost like a rigid body, because of the too complex shapes the blades have to acquire. The region of the diagram where two curves get close together is called *veering zone*. Here there is a mixing of the modes and they may be difficult to distinguish.

### 3.1.3 Modal Assurance Criterion

When studying the vibrations of a bladed disk, engineers may need a tool to compare the eigenvectors coming from different sources. The most common situation is when the results from a FE modal analysis must be compared against experimental data. In experimental modal analysis, modal parameters are obtained by measuring the *operating deflection shape* (ODS), which is defined as any forced motion of two or more points on a structure [20]. The motion values of the points of interest are obtained by externally exciting the body with an impulsive input generated by an instrumented hammer. Firstly the structure is set up with strain gauges or accelerometers, which locally measure the deformation of the structure and the acceleration of the body. Then, by means of post-processing techniques, it is possible to build the modeshapes and the natural frequencies. Another possibility is to use the tool to benchmark the results obtained with one software with respect to another one.

The most employed parameter to compare modal eigenvectors is the MAC (*Modal Assurance Criterion*). It is equal to 1 when the compared eigenvectors represent the same mode, 0 otherwise. It may also assume all the values between 0 and 1. Because of numerical errors, the setting of a threshold below which the modeshapes are considered different is needed, generally its value is set between 0.6 and 0.7. The MAC definition is given in equation 3.21

$$MAC = \frac{|\{\psi_T\}^T \{\psi_T\}^*|^2}{(\{\psi_T\}^T \{\psi_T\}^*) \cdot (\{\psi_S\}^T \{\psi_S\}^*)} \quad (3.21)$$

where the subscripts T and S state the numerical and experimental eigenvector respectively, the superscript T stands for the transpose matrix (i.e. the values in the columns of  $\{\psi\}$  are placed in the rows of  $\{\psi\}^T$ ), eventually the superscript \* means *complex conjugate* (i.e. the sign of the imaginary part is changed).

### 3.1.4 Cyclic Symmetry in FE Analysis

When modelling the dynamics of the bladed disk, it is often impractical to perform a FE analysis on the entire structure. Because of the large number of degrees of freedom involved, computer memory or nodes number limit in the software may make the analysis impossible. To solve this issue some *Reduced Order Modelling* (ROM) techniques have been developed in order to decrease the DoFs to be solved in the analysis. The FE models of the bladed disk make use of some geometric characteristics to reduce the number of nodes. The structure is rotationally periodic, i.e. it can be divided into N identical sectors, thus FE model can use the *Cyclic Symmetry*

boundary conditions [9] [2], allowing to compute the dynamic response of all the turbine stage just analyzing a single sector.

For cyclic symmetric bodies, the mass and stiffness matrices of equation 3.1, without considering the damping contribute, have a *block circulant symmetric* structure, when the vectors containing the DoFs and external excitation forces are organized such that n components of the first sector are followed by n components of the second sector and so on. A circulant matrix is a square matrix in which each row (after the first) has the same elements of the previous row shifted cyclically one place right [22].

$$[M] = \begin{bmatrix} [M_0] & [M_1] & [M_2] & \dots & [M_2] & [M_1] \\ [M_1] & [M_0] & [M_1] & \dots & [M_3] & [M_2] \\ [M_2] & [M_1] & [M_0] & \dots & [M_4] & [M_3] \\ \vdots & \vdots & \vdots & \ddots & \vdots & \vdots \\ [M_2] & [M_3] & [M_4] & \dots & [M_0] & [M_1] \\ [M_1] & [M_2] & [M_3] & \dots & [M_1] & [M_0] \end{bmatrix} \quad \{x\} = \begin{Bmatrix} \{x_1^S\} \\ \{x_2^S\} \\ \{x_3^S\} \\ \vdots \\ \{x_{N-1}^S\} \\ \{x_N^S\} \end{Bmatrix} \quad (3.22)$$

$$[K] = \begin{bmatrix} [K_0] & [K_1] & [K_2] & \dots & [K_2] & [K_1] \\ [K_1] & [K_0] & [K_1] & \dots & [K_3] & [K_2] \\ [K_2] & [K_1] & [K_0] & \dots & [K_4] & [K_3] \\ \vdots & \vdots & \vdots & \ddots & \vdots & \vdots \\ [K_2] & [K_3] & [K_4] & \dots & [K_0] & [K_1] \\ [K_1] & [K_2] & [K_3] & \dots & [K_1] & [K_0] \end{bmatrix} \quad \{F\} = \begin{Bmatrix} \{F_1^S\} \\ \{F_2^S\} \\ \{F_3^S\} \\ \vdots \\ \{F_{N-1}^S\} \\ \{F_N^S\} \end{Bmatrix}$$

where  $[M_i]$  and  $[K_i]$  (with  $i = 0, \dots, \text{int}(N/2)$  if N is even or  $i = 0, \dots, \text{int}((N-1)/2)$  if N is odd) are square matrices whose dimension is n.

Using the Fourier transform given in equation 3.23, the nodal displacement on all the nodes of the  $S^{th}$  sector can be expressed as a sum of cosine and sine components multiplied by the Fourier coefficients  $\{a_C\}$  and  $\{a_S\}$ , the subscripts denotes cosine and sine components [11].

$$\begin{aligned} \{x^S\} &= \frac{1}{\sqrt{N}} \{a^0\} + \frac{2}{\sqrt{N}} \sum_{h=1}^{\tilde{N}-1} \{a_C^h\} \cos((s-1)\psi) \\ &+ \frac{2}{\sqrt{N}} \sum_{h=1}^{\tilde{N}-1} \{a_S^h\} \sin((s-1)\psi) + \frac{1}{\sqrt{N}} (-1)^{s-1} \{a^{\tilde{N}}\} \end{aligned} \quad (3.23)$$

where N is the number of sectors and  $\tilde{N}$  is  $N/2$  if N is even or  $(N-1)/2$  if N is odd. In the second case the last term of the equation doesn't exist. Equation 3.23 also gives insight about the way blades vibrate. A vibration can be seen as the sum of

many contributes, one for each nodal diameter (h). Moreover the components with  $h \neq 0$  and  $h \neq N/2$  are harmonic functions over the disk.

A coordinates transformation from  $\{x\}$  to  $\{a\}$  allows the eigenproblem (equation 3.2) to be brought into a block diagonal form, so that N new cyclic symmetric eigenproblems can be solved separately [2].

$$\left( \begin{bmatrix} [\tilde{K}_0] & 0 & 0 & \dots & 0 & 0 \\ 0 & [\tilde{K}_1^C] & 0 & \dots & 0 & 0 \\ 0 & 0 & [\tilde{K}_2^C] & \dots & 0 & 0 \\ \vdots & \vdots & \vdots & \ddots & \vdots & \vdots \\ 0 & 0 & 0 & \dots & [\tilde{K}_2^S] & 0 \\ 0 & 0 & 0 & \dots & 0 & [\tilde{K}_1^S] \end{bmatrix} - \omega_i^2 \begin{bmatrix} [\tilde{M}_0] & 0 & 0 & \dots & 0 & 0 \\ 0 & [\tilde{M}_1^C] & 0 & \dots & 0 & 0 \\ 0 & 0 & [\tilde{M}_2^C] & \dots & 0 & 0 \\ \vdots & \vdots & \vdots & \ddots & \vdots & \vdots \\ 0 & 0 & 0 & \dots & [\tilde{M}_2^S] & 0 \\ 0 & 0 & 0 & \dots & 0 & [\tilde{M}_1^S] \end{bmatrix} \right) \begin{Bmatrix} \{a_0^C\} \\ \{a_1^C\} \\ \{a_2^C\} \\ \vdots \\ \{a_2^S\} \\ \{a_1^S\} \end{Bmatrix} = \{0\}$$

This way the eigenvectors and eigenvalues can be obtained for a specific nodal diameter without any approximation and considering the DoFs of just one sector. Indeed, solving the N eigenproblems corresponds to isolate the mode shape modulated by either the function  $\cos(h\theta)$  or  $\sin(h\theta)$ .

Taking into consideration the sector representing the whole structure (figure 3.8), two regions can be identified to be in cyclic symmetry: the faces of the disk and shroud. The vector containing the DoFs of the sector  $\{x^S(t)\}$  can be rearranged as follow:

$$\{x^S\} = \begin{Bmatrix} x_L^S \\ x_I^S \\ x_R^S \end{Bmatrix} \quad (3.24)$$

where a distinction has been made between internal and external points, the former are the ones not in common with adjacent substructures, on the contrary the sector shares the DoFs contained in  $\{x_L^S\}$  and  $\{x_R^S\}$  with neighboring sectors. External points are further divided into left and right nodes, depending on the position of the neighboring sector with respect to the fundamental one. The subscripts L and R represent this distinction.

Similarly the exciting force vector  $\{F\}$  can be organized as follow:

$$\{F\} = \begin{Bmatrix} F_L \\ F_I \\ F_R \end{Bmatrix} \quad (3.25)$$

Considering just one sector and neglecting the damping term, the equation of motion (equation 3.1) becomes:

$$([K^S] - \omega^2[M^S])\{x^S\} = \{F\} \quad (3.26)$$

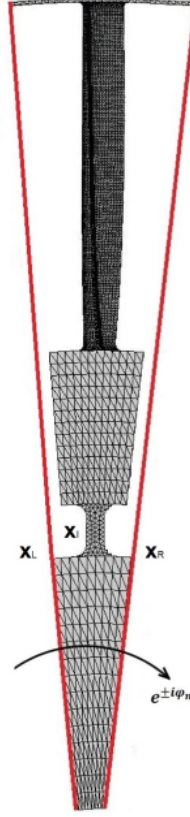


Figure 3.8: Fundamental sector of a bladed disk where the cyclic symmetry region is marked in red [3]

Considering a specific mode, the phase shift between neighboring sectors is fixed. Thus a relationship exists between the DoFs of the right and left external points. Since the behavior of neighboring sectors is out of phase of an angle equal to the IBPA, the following equation can be written.

$$\{x_R^S\} = e^{i\psi} \{x_L^S\} \quad (3.27)$$

In order to impose the cyclic symmetry boundary condition in the FE model, it is important to have corresponding meshes on the faces where the condition is set. With this condition applied, the DoFs vector becomes:

$$\{x^S\} = \begin{Bmatrix} \{x_L^S\} \\ \{x_I^S\} \\ e^{i\psi} \{x_L^S\} \end{Bmatrix} \quad (3.28)$$

The mass and stiffness matrices are reduced too, they assume different values on the

basis of the IBPA considered.

$$\begin{aligned} [K^S(\psi)] &= [T]^T [K^S] [T] = \begin{bmatrix} [I] \\ [I] \\ [e^{i\psi} I] \end{bmatrix}^T [K^S] \begin{bmatrix} [I] \\ [I] \\ [e^{i\psi} I] \end{bmatrix} \\ [M^S(\psi)] &= [T]^T [M^S] [T] = \begin{bmatrix} [I] \\ [I] \\ [e^{i\psi} I] \end{bmatrix}^T [M^S] \begin{bmatrix} [I] \\ [I] \\ [e^{i\psi} I] \end{bmatrix} \end{aligned} \quad (3.29)$$

The eigenproblem (equation 3.2) assumes the form:

$$([K^S(\psi)] - \omega^2 [M^S(\psi)]) \begin{Bmatrix} \{x_L^S\} \\ \{x_I^S\} \end{Bmatrix} = \{0\} \quad (3.30)$$

The solution of equation 3.30 depends on the value assumed by  $\psi$ . Setting the IBPA means finding the modes with a specific nodal diameter. Thus to retrieve all the mode shapes of the structure, it is necessary to solve the eigenproblem for all the possible values of  $\psi$  (equations 3.18 and 3.19).

## 3.2 Exciting Forces

The exciting forces on the bladed disk have an aerodynamic nature. Perturbations in the pressure field of the fluid may have different sources:

- the upstream stages generate wakes which impact on the blades of the rotor during their rotational motion;
- the downstream stages perturb the fluid pressure field. Their effects are large especially when the flux is transonic;
- the combustion chamber is the component just upstream of the turbine. The perturbations on the hot air caused by it have an effect especially in the high pressure turbine
- the *Inlet Guide Vanes (IGV)* is a static row of vanes which directs the flow toward the turbine, its repercussions on the fluid are similar to any upstream stage.

In addition to the aerodynamic forces, the bladed disk can be subjected to mechanical vibrations, due to not perfectly symmetric bodies. Because of the rotational velocity of the rotor, the excitation is periodic and resonance phenomena can take place when the excitation frequency is equal to one of the natural frequencies of the structure. The



rotational velocity  $\Omega$ , as well as the number of airfoils in the upstream and downstream stages, influence the excitation frequency. The parameter used to describe the exciting action on the bladed disk is the *Engine Order* (EO), which is the ratio between the pulsation of the exciting force ( $\omega$ ) and the rotational velocity of the disk. Since resonance always manifests itself at frequencies that are multiple of  $\Omega$ , the EO is an integer number.

$$EO = \frac{\omega}{\Omega} \quad (3.31)$$

### 3.2.1 Forward and Backward EO

The exciting action can be considered static, when it is seen from a steady reference system, or rotating, when the reference frame moves with the blades. In the last case the turbine stage is excited by two different rotating forces: one synchronous with the disk the other rotating in opposite direction.

The forces acting on the blades can be approximated as impulses. Even though their action last for a very small time, their duration is not negligible with respect to the revolution period of the disk. A simple example, very useful to understand the physics of the forced response, is displayed in figure 3.9. A disk with four blades is excited by a force acting at a specific angle ( $\theta^*$ ) along the circumference. The harmonic force is described by equation 3.32. The bladed disk, during its motion, encounters the force N times, where N is the number of blades.

$$\begin{cases} F_{\theta^*}(t) = F_0 \cos(\omega t) = F_0 \cos(N\Omega t) \\ F_{\theta \neq \theta^*}(t) = 0 \end{cases} \quad (3.32)$$

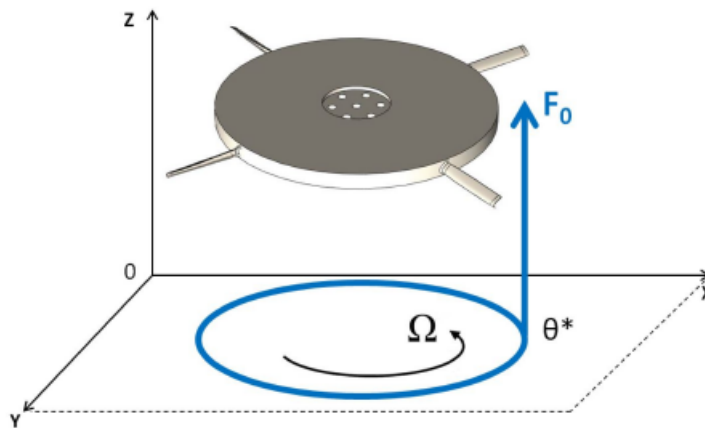


Figure 3.9: A disk with 4 blades excited by an harmonic force [6]

The harmonic force can be decomposed, with respect to a static frame, along the circumferential coordinate using the Fourier transform [3]. It assumes the following form:

$$F_{\theta,Fix}(t) = \frac{F_0}{\pi} \sum_{n=0}^{\infty} \cos(n(\theta - \theta^*)) \cos(\omega t) \quad (3.33)$$

where  $n$  is the harmonic index. To transform equation 3.33 in the rotating frame, a variable change is needed ( $\theta = \theta_R + \Omega t$ ) and the equation becomes:

$$F_{\theta,Rot}(t) = \frac{F_0}{2\pi} \sum_{n=0}^{\infty} [\cos((\omega - n\Omega)t) \cos(n\theta_R) + \sin((\omega - n\Omega)t) \sin(n\theta_R) + \cos((\omega + n\Omega)t) \cos(n\theta_R) - \sin((\omega + n\Omega)t) \sin(n\theta_R)] \quad (3.34)$$

here the two rotating forces are distinguishable, they are portrayed in figure 3.10. Their pulsations are:  $\omega_f = \omega - n\Omega$  (forward exciting force) and  $\omega_b = \omega + n\Omega$  (backward exciting force).

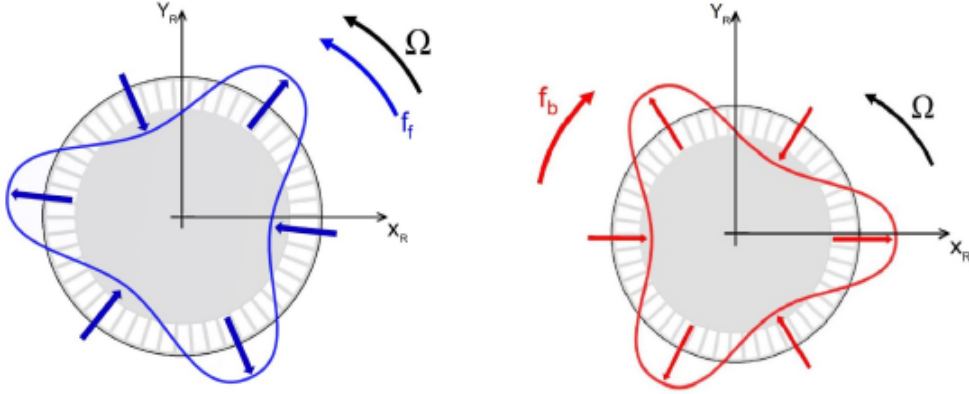


Figure 3.10: On the left a forward rotating force, on the right a backward rotating force with harmonic index  $n = 3$  [6]

Considering the example of figure 3.9 and assuming the harmonic index to be 2, the structure is excited by two different EO at the same time. They can be computed as follow:

$$\begin{cases} \omega_b = \omega + n\Omega = \Omega(N + n) = 6\Omega = EO_b\Omega \rightarrow EO_b = \frac{\omega_b}{\Omega} = 6 \\ \omega_f = \omega - n\Omega = \Omega(N - n) = 2\Omega = EO_f\Omega \rightarrow EO_f = \frac{\omega_f}{\Omega} = 2 \end{cases}$$

where  $EO_b$  and  $EO_f$  are the Engine Orders exciting the structure in the rotating reference system. On the contrary, in the static reference system, there is just one EO:  $EO = 4$ .

### 3.2.2 Campbell Diagram

Dr. Campbell, working at the *Rotor Dynamics Laboratory* of the vapor turbine plant of General Electric in Schenectady, developed an effective way of representing the resonance conditions of the turbine blades: the *Campbell Diagram* (figure 3.11). On the x-axis of the diagram is the rotational velocity of the disk, while the frequency lays on the y-axis. On the plot both the natural frequencies of the modes and the frequencies of the exciting forces are represented. The latter are oblique lines starting from the origin of axes, with a slope equal to the EO, as it can be easily seen from equation 3.31. The crossings between modes curves and EO are potential resonance conditions, their danger is given by the level of amplification and by the amount of time the engine spends rotating at that particular rotational velocity. Thus the most hazardous ones are the ones inside the operative range of the engine, they require some further investigation to see if resonance phenomena are actually strong enough to lead to the rupture of the structure.

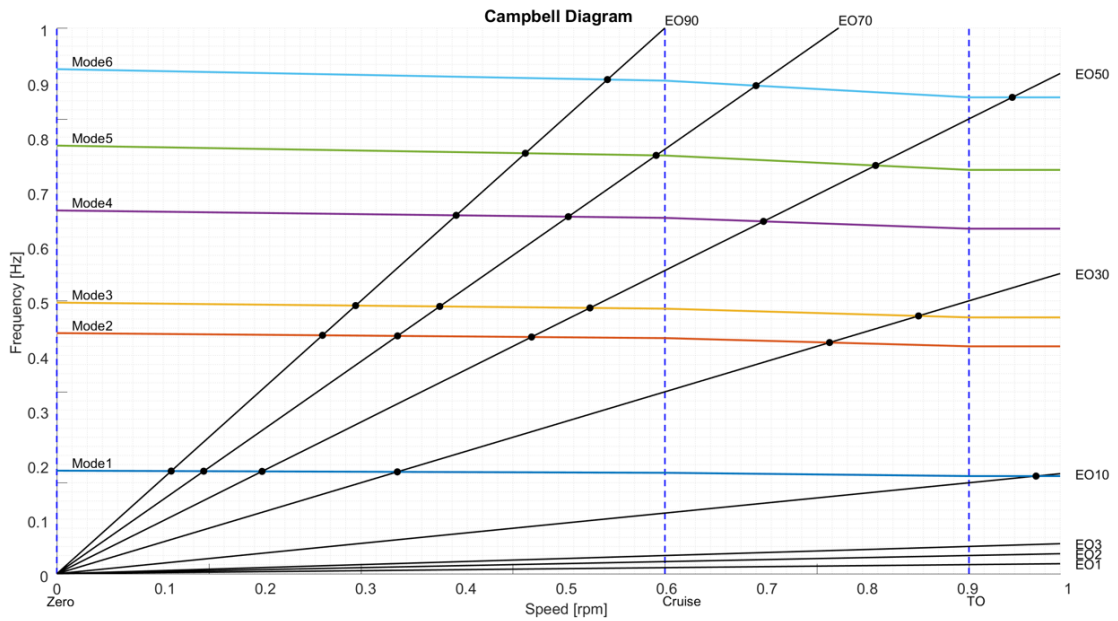


Figure 3.11: Campbell Diagram

The natural frequencies of the modes change over the rotational velocity range because of two main effects: the stiffening due to the centrifugal load and the softening due to the temperature distribution, which alters the material properties. Indeed at different throttle settings both the rotational speed and the temperature change. Usually the softening effect prevails, leading to decreasing curves.

### 3.2.3 Resonance Conditions

As already mentioned resonance presents itself when the exciting force frequency matches the natural frequency of the structure. Still not all the crossings of the Campbell diagram represent a resonance condition. Let's consider a generic mode  $y$  with a certain natural pulsation  $\omega_n$  and nodal diameter.

$$y(t, \theta) = -y_n \cos(\omega_n t + ND\theta) \quad (3.35)$$

where  $\theta$  is the angular coordinate. No hardening effects are considered, so the mode frequency doesn't change with the rotational velocity of the disk ( $\Omega$ ).

During its rotation, the bladed disk is subjected to periodic forces that can be decomposed into their harmonics using the Fourier transform.

$$f(t, \theta) = f_0 + \sum_{k=1}^{\infty} F_k \sin(k(\omega t + \theta)) \quad (3.36)$$

where  $F_k$  is the amplitude of the  $k^{th}$  harmonic and  $\omega$  is the exciting force pulsation, which is multiple of the rotational velocity. The work made by the exciting harmonic on a mode with nodal diameter ND over a period T is defined as follow:

$$\int \int f dy d\theta = \int \int f \frac{dy}{dt} dt d\theta = \int_0^{2\pi} \int_0^T f(\theta, t) \frac{\partial y(\theta, t)}{\partial t} \frac{\Omega}{2\pi} d\theta dt \quad (3.37)$$

When work is positive, energy piles up and the resonance condition is met. Substituting  $f(\theta, t)$  and  $y(\theta, t)$  and solving the equation, the mathematical formulation of the resonance condition can be found:

$$W = \begin{cases} \Omega \pi F_k y_n & \text{if } \omega_n = k\omega \text{ and } ND = n \\ 0 & \text{if } \omega_n \neq k\omega \text{ and } ND \neq n \end{cases} \quad (3.38)$$

In equation 3.38 the circumstances under which resonance condition manifests are written. The first one, which states that the natural frequency of the mode must be equal to a multiple of the exciting force frequency, is the classic one, while the second condition states that the exciting harmonic index must be equal to the nodal diameter. Both these requirements must be met in order to have resonance. The relationship that links EO and ND under resonance condition is given in equation 3.39, where  $N_b$  is the number of blades in the stage.

$$\begin{cases} EO = ND \\ EO = N_b \pm ND \end{cases} \quad (3.39)$$

Equation 3.39 can be rewritten in the following compact form:

$$EO = mN_b \pm ND \quad \forall m \in \mathbb{N} \quad (3.40)$$

When the Engine Order is equal to the nodal diameter, the shape of the exciting force is the same as the mode shape, thus the points of maximum force correspond to the points of maximum deflection and, if the excitation frequency matches the natural frequency of the mode, resonance manifests. The same exciting action won't have the same effect on all other modes, since its shape is orthogonal to them. The condition expressed by the second case of equation 3.39 depicts the *aliasing* phenomenon. The blades are not a continuous system along the angular coordinate of the bladed disk, they sample the exciting force in a finite number of points. For certain values of EO, the structure sees a different frequency than the actual one and the "perceived frequency" may comply with the resonance condition expressed by the first case of equation 3.39. Figures 4.1 shows the aliasing phenomenon on a disk with 32 blades excited by an EO equal to 24 (green curve). The structures perceives the exciting action as it had EO = 8 (blue curve). Another way to identify what ND is excited

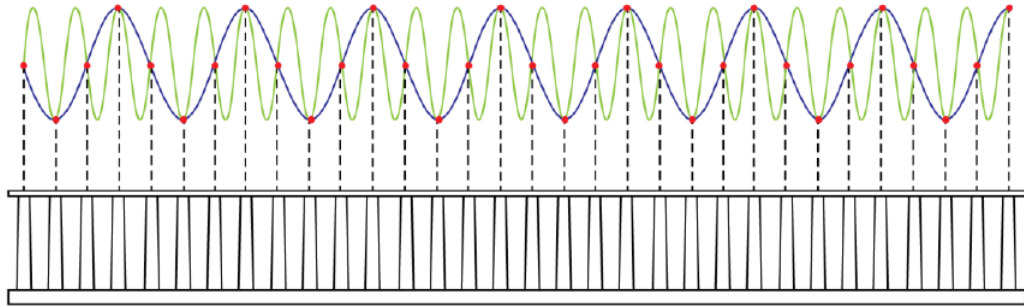


Figure 3.12: Aliasing phenomenon [24]

by a specific EO is given by the following algorithm [24]:

$$N_{waves} = \frac{EO}{N_{sect}}; \quad N_{waves,INT} = INT\left(\frac{EO}{N_{sect}}\right)$$

$$N_R = EO - N_{waves,INT} \cdot N_{sect}$$

$$\begin{cases} H = N_R & \text{if } N_R < \frac{N_{sect}}{2} \\ H = N_R - N_{sect} & \text{if } N_R > \frac{N_{sect}}{2} \end{cases}$$

For example, considering a bladed disk with 11 blades excited by an  $EO = 100$ .  $N_{waves} = 9.09$  is the number of waves in a sector. Thus, along the sector, there are 9 complete waves and a surplus of almost one tenth of a wave. Had  $N_{waves}$  been exactly 9, because of the aliasing phenomenon previously described, the perceived EO would have been 0. But, since the substructure doesn't contain an integer number of waves, assuming the exciting action has a cosine shape on the sector, the EO starts with maximum amplitude and ends with lower amplitude (figure 3.13). The step further in the cosine function has a value of  $Alfa = 0.09 \cdot 2 \cdot \pi = 32.72^\circ$ , it is contained eleven times in the full circle:  $32.72^\circ \cdot N_{sect} = 360^\circ$ . Thus the exciting wave perceived by the structure completes one cycle over the disk and the nodal diameter excited by this wave is  $ND = 1$ . The same conclusion can be achieved by using equation 3.40 with  $m = 9$ .

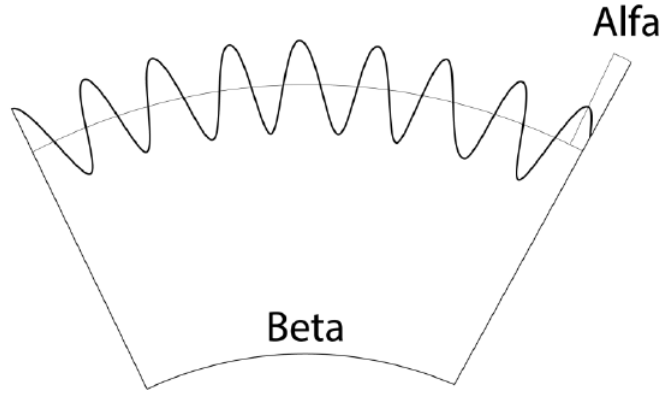


Figure 3.13: EO on a sector [24]

# Chapter 4

## LPT Design

The design of a Low Pressure Turbine is a complex procedure which involves two main disciplines: aerodynamics and structural mechanics. The former has the goal to maximize the efficiency of the blade, i.e. the conversion of the energy contained in the flow, in the form of pressure and velocity, into mechanical power on a shaft. While structural mechanics studies the resistance of each components under static and dynamic loads. Moreover, the interaction between fluid and structure must be studied. Potential unstable vibratory phenomena sustained by the airflow can manifest under certain conditions, flutter analyses are performed to guarantee that these conditions are outside the operative range of the engine.

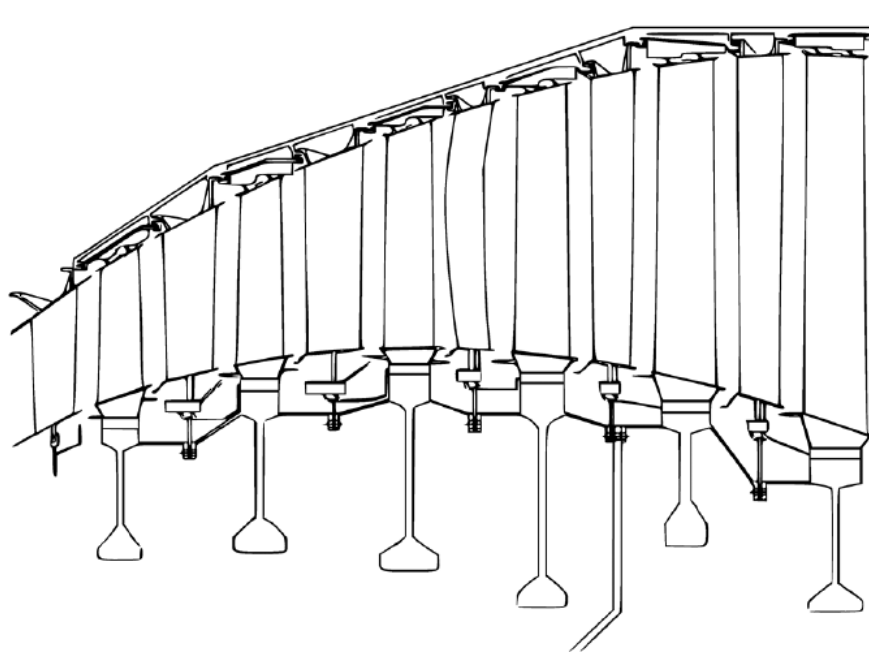


Figure 4.1: LPT cross section [10]

The preliminary design of LPT needs some information as inputs, which are derived from the conceptual design of the whole engine:

- broad measures of the engine;
- rough cross section based on the global inlet/outlet pressure drop;
- power output.

## 4.1 Aerodynamic Design

As already mentioned, the main goal of the aerodynamic design is the definition of the airfoil which represents the optimum for the energy conversion from fluid to mechanical power. The first step is the definition of the turbine *flowpath*. At a certain working condition or *design point*, the flowpath is the channel traveled by the air flow while expanding. It is represented on a 2D-sketch (figure 4.2) by a collection of *corner points* representing the projection on the engine cross-section of the maximum size of the vane or rotor blade aerodynamic profile [4]. Succeeding the flowpath definition,

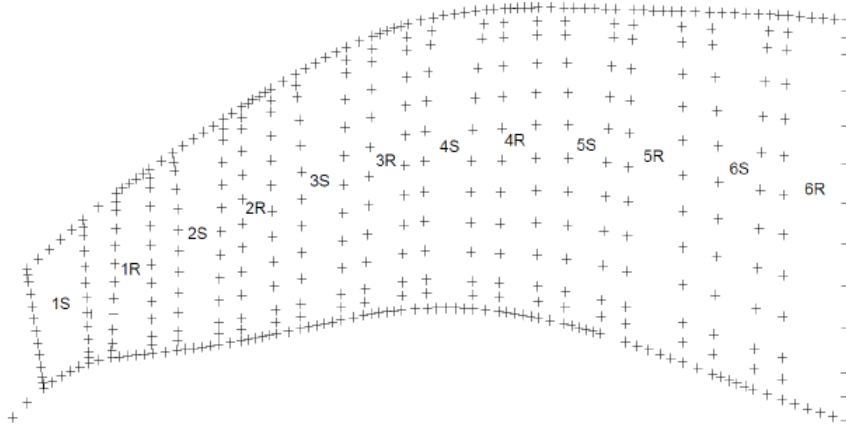


Figure 4.2: 2D-sketch of the flowpath of a 6 stages LPT. The corner points are identified by the symbol (+). R stands for rotor and S for stator [4]

blades are designed in working condition (hot condition). To determine the profile of the blade, a three step process is followed[10].

- 1- *1D Optimization Process*: in order to comply with the requirements coming from the conceptual design of the engine, the LPT is divided into stages, since a single stage can't produce a pressure drop large enough to match the global



inlet/outlet pressure ratio. Each stage is further subdivided into sectors. The fluid path through the machine is represented by *velocity triangles* (figure 4.3). They are used to determine some features of the bi-dimensional airfoils (such as leading and trailing edge orientation), which represent to the blade cross-sections from the root to the tip. To ensure equal work done by the air flow along the length of the blade, different stagger angle values are employed at different radial locations (figure 4.4).

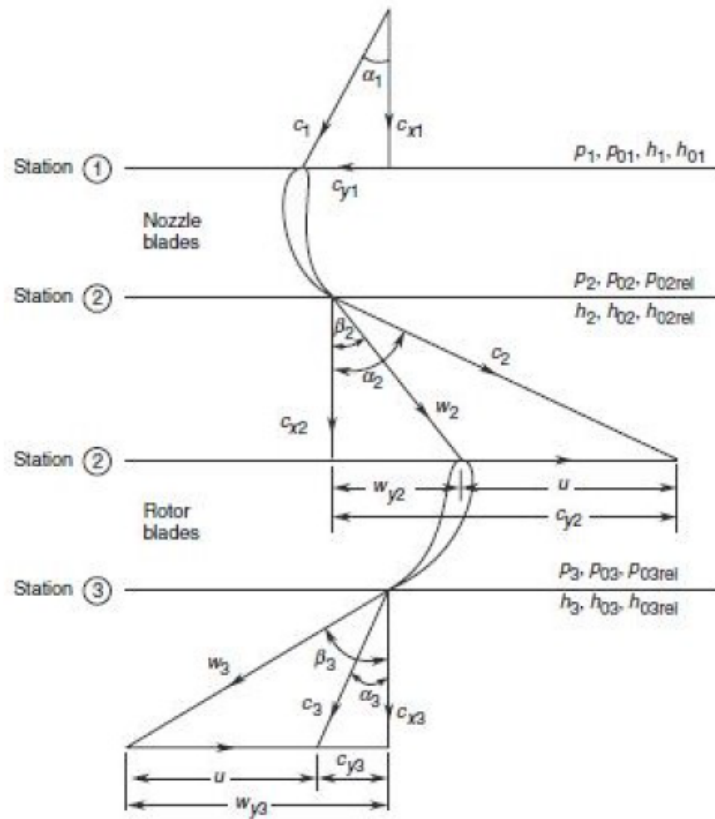


Figure 4.3: Velocity triangles of a LPT stage. The speed in the steady reference system is  $c$ , while  $w$  represents the velocity in a coordinate system rotating with the rotor. In order to achieve the optimal flowpath, the air must be deflected in specific directions, thus determining the leading and trailing edges geometry. [10]

**2- 3D profile:** the outcomes of the 1D design are elaborated through a number of empirical correlations, coming from the AvioAero know-how, in order to build the 3D shape of the airfoil that best fulfill the performance requirements. Once the airfoil is ready, CFD (*Computational Fluid Dynamics*) analyses are performed

on all the stages (multi-rows) to determine the turbine response. The results obtained will be used to set some boundary conditions and loads in the next optimization loop.

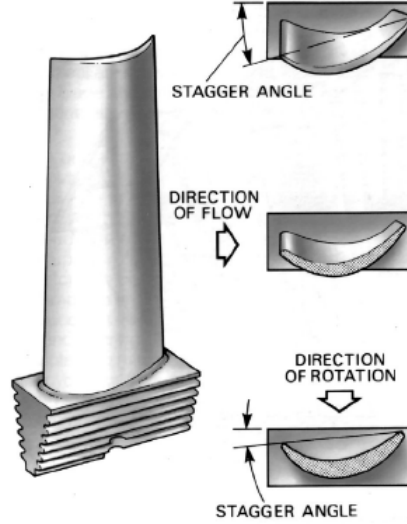


Figure 4.4: Turbine blade showing twisted contour [4]

- 3- *Optimization*: once the best shapes are selected, which respect the BCs and comply with the performance requirements, they are frozen and studied more in detail. Their geometry is investigated in terms of leading and trailing edge, chordal length (i.e. axial extension of the airfoil), thickness distribution. The variations are limited to a small percentage of the base geometry, the performance trends are plotted and the best configuration is frozen as *Aero Pass*, and will be further analyzed from a mechanical point of view.

## 4.2 Structural Design

Before structural analyses can be performed, the CAD must be completed with outer and inner elements. As seen in chapter 1.2.1, to the standard vane configuration are attached IBV and OBV, while for the standard rotor blade the elements to be appended are dovetail or firtree, shank and shroud. Nevertheless the contra-rotating turbine may require different geometries to be used.

As aforementioned, the blade profile is determined in hot condition. Still, the turbine is assembled in cold condition and it has to guarantee the correct positioning of

the airfoil in operating conditions, in order to realize the designed flowpath. This leads to the *hot to cold scaling*, needed for scaling the profiles from hot to cold condition. It consists in three operations:

- *Scaling*: scale reduction of the designed profiles by removing thermal expansion due to high temperatures.
- *Twisting*: to obtain the blade in cold condition, the designed cross-sections must be twisted around their radial direction.
- *Positioning*: defines the position of the elements needed to keep fixed the airfoil.

Once the geometry is defined, a FE model is built and the mechanical behavior of the structure is simulated on software. The main structural analyses conducted at this level are: the modal analysis, to study the dynamics of the system and its vibratory behavior, and the static analysis, to get the static deformation and stresses due to loads such as pressure coming from the air flow, centrifugal load (just in the case of rotor blades), thermal load and pre-twist.

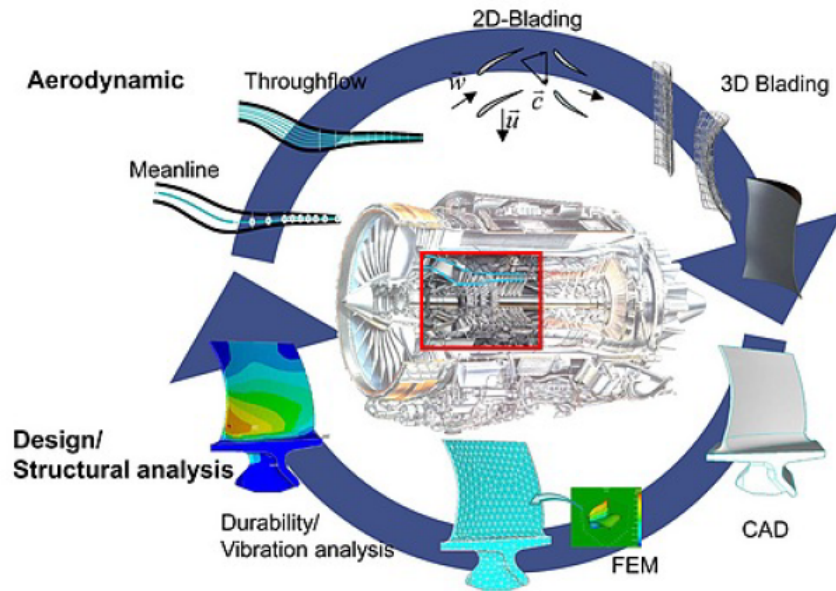


Figure 4.5: Traditional design workflow for LPT stages [10]

If the mechanical simulation forecasts the rupture of the structure, the airfoil is sent back to the aerodynamic team for further modifications. After a new geometry is developed, mechanical analyses are run again. The loop continues until good results

are obtained from a structural point of view. Afterwards more detailed analyses are performed, such as the Campbell diagram generation, to assess the turbine response over a large range of conditions. The forced response is further investigated in those operative conditions that may lead to resonance phenomena. Finally the flutter analysis is performed, to study the interaction between fluid and structure. At this point the geometry is definitively frozen for manufacturing.

The main problem in the traditional design workflow for LTP stages is that further detailed analyses are conducted after the geometry has been consolidated, for instance the fatigue limit study. So, if the safety factors are not met, improvements of the structure can only be made by local modifications and fixing. Moreover the process is made of two separate optimization loops, one for the aerodynamics behavior, one for the mechanical response, thus not leading to a global optimum. What is good for one aspect, may not be good for others.

### 4.3 Aero-Mech Design

To overcome the issues mentioned in the previous chapter, a new design process is required, which, conversely to the traditional design, takes into consideration the mechanical requirements of the structure in the early stages of the design process: the *Aero-Mech Design*. This thesis has its final goal in the development of a tool (PRIME) that can make this concept possible.

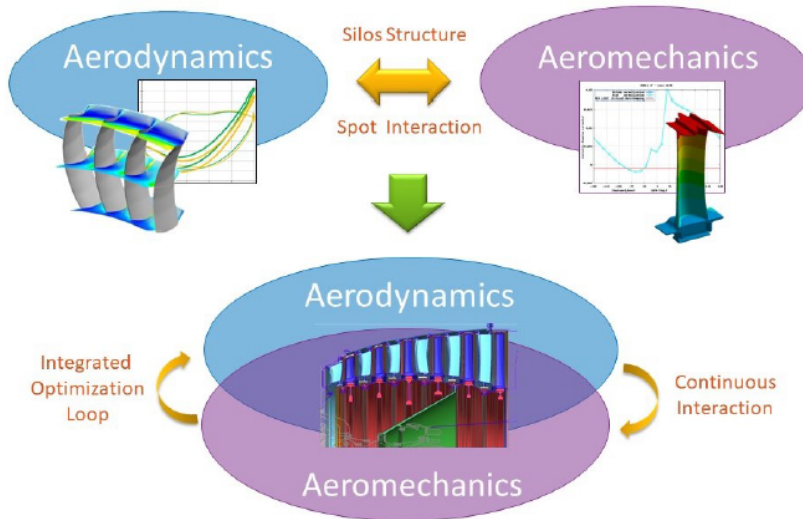


Figure 4.6: Aero-Mech design representation [10]

The main purpose of the PRIME tool is to anticipate at preliminary level some more detailed analyses and include in the first optimization loop (the generation of the 3D airfoil) some mechanical thresholds, in order to find the right trade-off between aerodynamic and structural requirements. To accomplish this goal, the PRIME tool must comply with the following conditions:

- it must provide the aerodynamic designers with a mechanical feedback, through the production of easy to understand outputs. Since the tool generates a large amount of information, a clear way of showing them is needed. All data will be available on a dashboard, with which the user can interact in order to obtain the information he needs. Moreover quality indexes will be defined, to give the user an easy and immediate way to assess the goodness of the analyzed configuration. This will allow the optimization of blade profiles considering not only the increment of performance, but also the mechanical characteristics of the structure.
- the process must be automatic. This way it will be quicker and accessible to all users, even the less experienced ones. It is very important for the tool to be user-friendly, since it is thought to be mostly used by aerodynamic designers, who may not have a deep insight in what the structural issues are and how the structural analyses are conducted.
- the tool will be able to run all the structural analysis automatically, in the case the user wants an overall understanding of the mechanical behavior of the structure. Furthermore, the user will be able to select specific analyses, when just some particular information are needed.
- the definition of a global process, in order to reduce possible time losses and avoid misunderstandings while exchanging information.

The construction of the tool takes advantage of interesting features of the software Ansys Workbench, which allows the process to be relatively easily automatized. The reduction of computation time attainable with this automatic procedure makes possible the running of detailed analyses during the preliminary design, thus leading to an optimization loop able to take into account mechanical issues as well as aerodynamic performances.

In figure 4.7 the PRIME workflow is displayed. All the routines which are part of the process are enlightened, as well as the connections between them. The focus of the present work is places in the static analysis and the forced response.

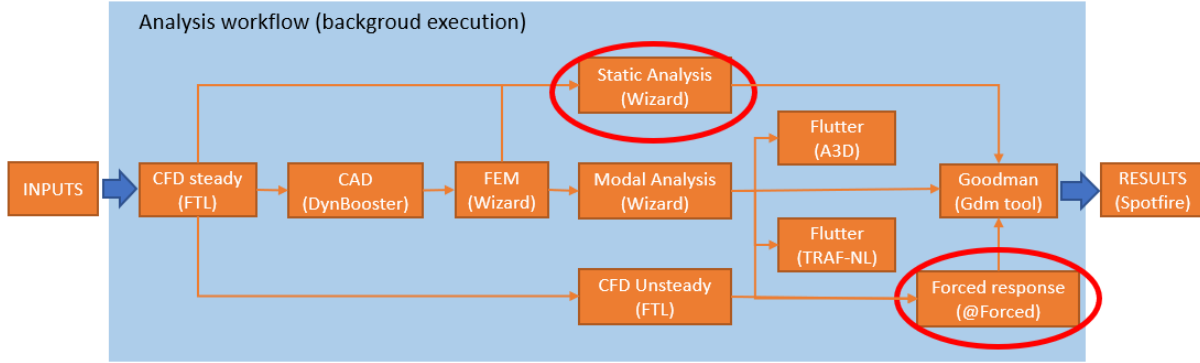


Figure 4.7: PRIME process. The focus of this thesis is placed in the building of the blocks encircled in red

### 4.3.1 PRIME Today

The tool is made of many routines written in different programming languages. Up to the moment this work is published many functionalities have already been implemented, each of them can run individually, but the frame that will link everything together have yet to be implemented. The functionalities developed so far are:

- *Generation of the CAD*: starting from aerodynamic inputs, the 3D airfoil is created, then the CAD is completed adding the inner and outer elements. These elements are managed using parametric templates, which the user can easily modify by changing a few numbers. The user can also choose what kind of templates to attach to the AF. This feature is especially useful when experimenting innovative configurations.
- *FEM model generation*: the mesh is automatically built and loads and boundary conditions are applied. The user can choose what structural analysis to run.
- *Static analysis*: all load cases and BCs are implemented for this kind of analysis, but, before it can be performed, the peanuts plots must be computed. They are used to know the amount of interference between two adjacent blades, due to the pre-twist of the structure (this matter is explained extensively in chapter 4.1.4).
- *Modal analysis*: a static analysis considering just the effects of temperature and inertial load is performed and the results are used as a pre-stress condition for the modal analysis. After modeshapes and natural frequencies are computed, a

report is generated for future flutter and forces response analyses. The principal output of the free response calculation is the Campbell diagram.

- *Flutter analysis*: this analysis is performed in order to obtain the plot of the aerodamping. It gives information about the stability of flutter phenomena, if the aerodynamic damping parameter assumes values below 0, the structure can incur into instability.
- *Forced response*: it combines aerodynamic and free response information to compute the work done by the aerodynamic exciting force on a specific mode. Eventually a parameter called *Modal Force* is computed. A large value of modal force indicates the energy is stacking up and the structure incur into dangerous resonance phenomena.
- *Post Processing of Data*: the user is given an easy way to access all data produced by the analyses. All plots and information are accessible through a dashboard.

Up to this moment the models processed by PRIME are the vane model and the *Blade Only model*: the disk is neglected and the blade is rigidly fixed at its base. It is a simplified model, since it doesn't take into account the interactions between blade and disk and it doesn't need cyclic symmetry boundary conditions. Still it is good enough for preliminary design and it has the advantage of having lower computational costs (the model is further discussed in chapter 4.2).

### 4.3.2 PRIME in the Future

As already mentioned, the PRIME tool is not yet complete. The next steps in its implementation are:

- The inclusion of disk templates in the CAD generation process, so that a bladed disk can be modeled.
- The developments of all FEM model of the bladed disk, with the appropriate conditions at the interface between the two solids.
- The inclusion in PRIME of the tool for the Haigh diagrams (used to analyze High Cycle Fatigue phenomena).
- The construction of the frame that will manage all the routines.





# Chapter 5

## Static Analysis

The loads a structure is subjected to are divided into three categories: the *static loads* are time independent, both their magnitude and direction never change, the *quasi-static loads* are generated by dynamic phenomena, but they evolve so slowly with respect to the overall time studied that they can be considered constant, finally the *dynamic loads* are time dependent and give birth to vibration phenomena. The quasi-static loads the bladed disk has to withstand during its operational life have four main sources. Due to the airflow passing over the blade profile, different pressures act on the suction and pressure side of the airfoil, causing a bending moment. The rotation of the structure leads to a centrifugal load. Since the gases coming from the combustion chamber are hot, the LPT stage sees a thermal gradient along specific directions. Eventually, when the turbine is assembled, the blades are mounted with a pre-twist about their radial axis. All these loads act on the LPT with almost constant magnitude and direction, given the operational condition of the engine. It is extremely important to evaluate the effects of these loads on the bladed disk, since they can cause displacements in the structure that may lead to interference problems with neighboring bodies, moreover they lead to internal stresses that may cause the structure to fail, when the stress limits of the materials are exceeded. The static analysis has the purpose to study the effects of the quasi-static loads acting on the structure.

### 5.1 Loads Acting on the Blade

In this section the quasi-static loads acting on the bladed disk are further discussed and analyzed.

### 5.1.1 Inertial Load

The LP shaft is characterized by high rotational speed, thus the inertial load is the principal one acting on the structure. The centrifugal force that a cross-section at a given radius  $r$  have to withstand is given in equation 5.1, where  $R$  is the maximum blade radius,  $\rho$  the material density,  $\omega$  the rotational velocity and  $A$  the cross-section area.

$$F_C = \int_r^R dF_C = \rho\omega^2 \int_r^R r \cdot dV = \rho\omega^2 \int_r^R r A(r) \cdot dr \quad (5.1)$$

It is evident that the section most suffering the centrifugal load is the blade root. In order to prevent its failure an appropriate design of the shank must be carried out, in particular the fillet joining the blade root with the shank platform plays a key role in this issue.

### 5.1.2 Pressure Load

The hot gases passing through the turbine exert a pressure field on the blade surface. Since the airfoil is designed to extract energy from the fluid and put the shaft into rotation, in order to collect mechanical power, the pressure fields on the pressure and suction side of the AF are different, giving birth to an overall action that makes the blade rotate. In addition to this effect, since the blade is clamped at its root, the

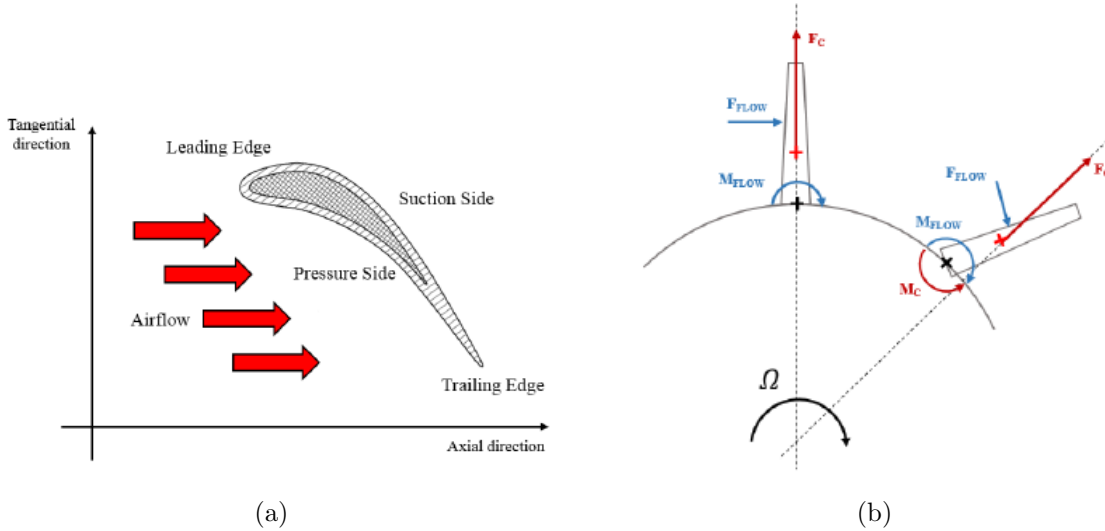


Figure 5.1: In figure (a) the cross-section of a turbine blade is shown, where the action of the airflow is represented by red arrows. In figure (b) a sketch of the working principle of camber practice is displayed [4]

structure is also subjected to a bending moment  $M_{FLOW}$ , which causes large stresses

in those areas where the blade is constrained: its root and possibly its tip, depending on the interlocking condition (i.e. the blade behaves as a clamped-free or clamped-clamped beam under the action of a distributed load). In order to attenuate the effect of the bending moment, the blade is skewed in the flow direction. The airfoil is tilted of 1 or 2 degrees with respect to its center of gravity, such that a new moment  $M_C$  is generated by the action of the centrifugal force, it acts in the opposite direction of  $M_{FLOW}$ . This practice is called *camber*, a sketch of how it works is shown in figure 5.1(b). The mechanical equilibrium of the two moments is achieved only under specific operating conditions, in all other cases,  $M_C$  will decrease but not completely eliminate the effect of the bending moment.

### 5.1.3 Thermal load

The hot exhaust gases coming from the burner causes thermal expansion on the LPT stages. The engine's components experience a thermal strain effect  $\epsilon_T$  that is proportional to the difference between the hot gases temperature and the reference temperature at which the material thermal expansion is considered null ( $T_0$ ).

$$\epsilon_T = \alpha(T - T_0) \quad (5.2)$$

Where  $\alpha$  is the coefficient of thermal expansion.

A temperature change doesn't lead to stresses in a component that is free to expand. However the bladed disk is constrained and thermal stresses occur. For instance, shrouded turbine blades may behave as clamped-clamped structures when the twist-back moment due to the centrifugal load enables a tight contact between adjacent interlocking faces.

Besides the thermal expansion, another phenomenon associated with high temperature working environments is *creep*. It generally occurs when a structure is exposed to a load for a long time. Even though the stress level is below the yield strength of the material, the component deforms permanently. Creep is more severe in materials that are subjected to heat. This is the case for turbine blades, which have to withstand a permanent centrifugal and pressure load under high working temperature.

Because of the high temperature, the material choice is critical, especially for the first rows of LPT blades. Cooling systems have been developed to overcome the problem. Cold air is spilled out from the compressor and is forced to pass through a series of ducts realized inside the airfoil (figure 5.2).

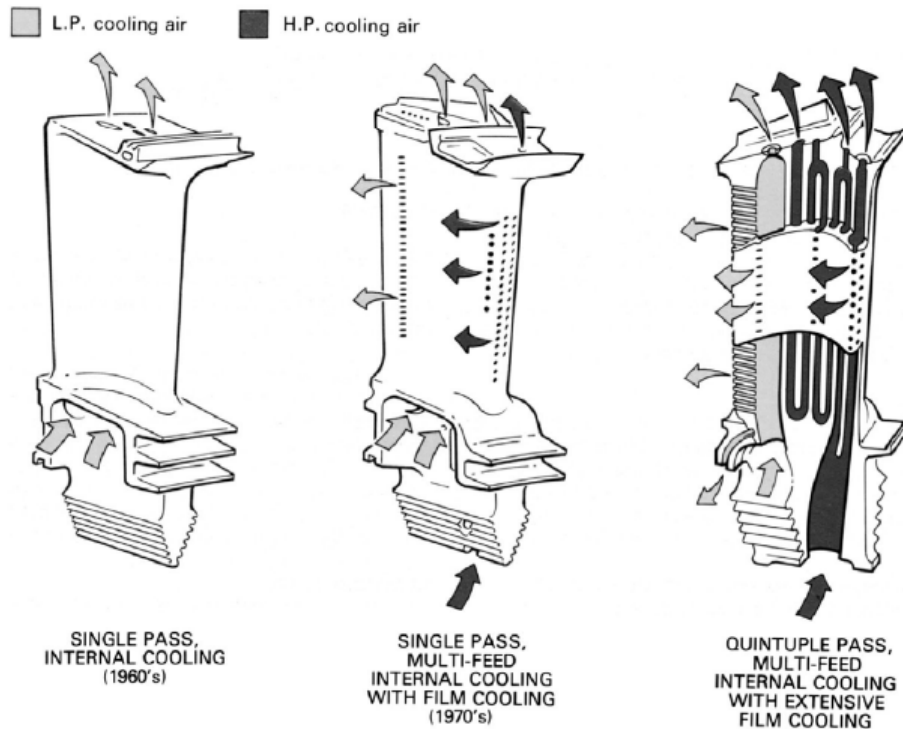


Figure 5.2: Development of turbine blade cooling [19]

#### 5.1.4 Pre-Twist

When assembling LPT stages the blades are pre-twisted around their radial axis [18]. Because of the twisting effects due to operational loads on the blade, the pre-twist is needed to assure an optimal positioning of the AF with respect to the flow. Analyzing a single blade, it is subjected to the action of the neighboring sectors, which push the shroud of the analyzed structure (as shown in figure 5.3) until there is no more interference.

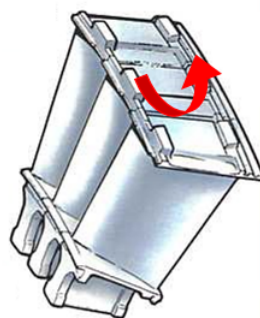


Figure 5.3: Pre-twist effect on the blade

Two main factors have an influence on the interference value:

- Temperature gradients make the shroud expand, increasing interference.
- The centrifugal load stretches the blade along the radial direction, bringing the blade tip to a larger circumference, thus decreasing interference.

*Peanuts plots* are used to display the amount of interference at different operating conditions of the engine. Interference can also be measured as a force or a moment acting on the shroud. An example is given in figure 5.4, the blue curve is for the engine while accelerating, since it starts from cold condition, its temperature is lower and so is the interference value. On the contrary the red curve represents decelerating conditions.

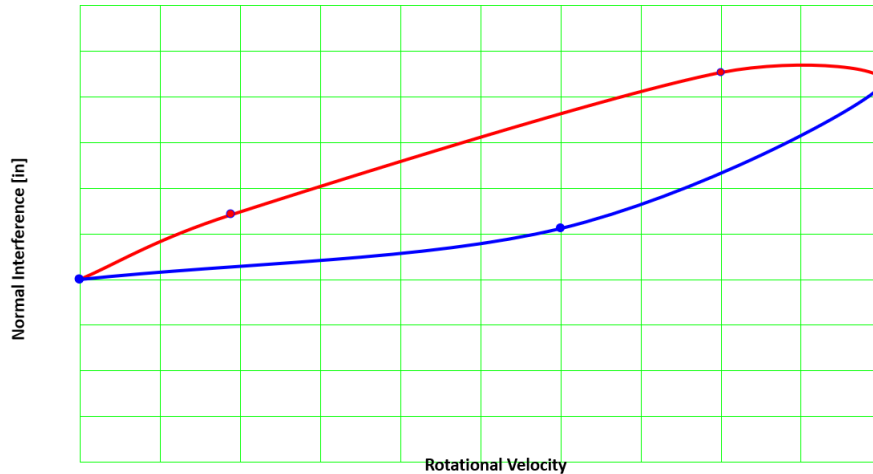


Figure 5.4: Peanuts plot example

## 5.2 Static Analysis in PRIME

The static analysis implemented in PRIME takes into consideration all the loads previously described. The analysis is applied to a blade only (BO) model. This is a simplified model where the disk is not included, instead of having a coupling of the contact nodes between the two bodies, an external boundary condition is needed to keep the blade in place. This assumption is valid in those cases where the movement of the disk is very small, for instance in modal analysis the modes on the FREND diagram asymptote comply with this requirement. For a static analysis this may be a strong simplification, but it is still good enough for preliminary design, where there

is no need to have detailed information on the stresses acting on the blade, since the geometry is still rough. What engineers are after in this stage of design is the general behavior of the structure, they look for areas where there is a large unbalance of forces. The BO model doesn't need cyclic symmetry boundary conditions.

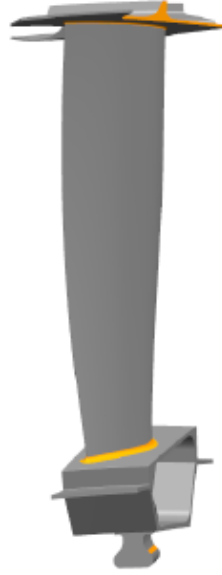


Figure 5.5: Blade Only model with important surfaces for FE analysis enlightened [12]

FE analyses in PRIME are performed in Ansys Workbench. The results are validated against msc Nastran, which is the software where Avio Aero legacy is built upon. Once the model has been set up and solved in NS, considering the design practice of the company, the mesh and materials are imported into WB. Here all loads and BCs must be introduced again, finding the best settings which are most similar to the NS ones. The difference in results is computed on every nodes and is shown as a percentage (%err):

$$\%err = \left| \frac{u_{NS} - u_{WB}}{u_{NS}} \right| \cdot 100 \quad (5.3)$$

where  $u_{NS}$  is the Nastran result and  $u_{WB}$  is the Workbench result. The results considered are directional displacements and the maximum principal stress. Principal stresses are the components of the stress tensor when it is rotated in such a way that the shear stresses are null. The maximum principal stress is the maximum between these three values.

When the absolute value of the results becomes smaller, the percent difference grows, still the absolute difference may stay small, not affecting the goodness of the solution. For this reason a filter has been used to exclude all nodes whose results are at least three order of magnitude smaller than the maximum value.

The results presented in this chapter are calculated on the airfoil, since the aerodynamic team the PRIME tool is thought for are mostly interested in understanding the behavior of the blade profile. Moreover the AF is far enough from the boundary conditions, thus it is not affected by their effects, making the validation results easier to understand. The AF is divided into ten spans along its radial direction, for each section the average %err and the maximum absolute difference (dif) are computed. The last quantity is normalized with respect to the maximum value of the results.

### 5.2.1 Ansys Elements Investigation

Before building the analyses on a complex structure such as a turbine blade, a simple cantilevered beam model has been created in order to study how Ansys elements behaves in presence of many different loads (figure 5.6): a forced applied at the unconstrained end of the beam, centrifugal load, thermal load, pressure load and twist, applied through two forces at the beam tip.

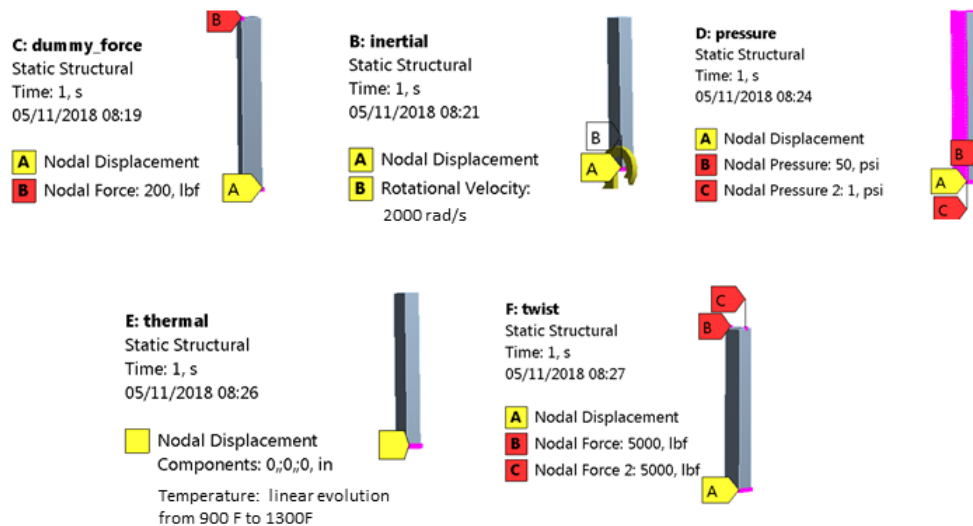


Figure 5.6: Loads analyzed for the cantilevered beam model.

At first a comparison has been made between Ansys Workbench and Ansys APDL (a software used by some Avio Aero businesses), in order to understand all the parameters at stake in element formulation and to find out what default conditions are

applied by WB. Once WB settings are made identical to APDL ones, the second order tetrahedral elements can be compared to the Nastran ones. In table 5.1 the results are listed after the filter on the order of magnitude has been applied. The inertial load gives large errors for stresses at the beam tip, where they should approach 0. Because of the low stress level in this region, the last row of elements has been excluded from the stress results of the inertial case.

	NS --> WB filtered							
	X - displ		Y - displ		Z - displ		MaxP	
	%MAX	%AVG	%MAX	%AVG	%MAX	%AVG	%MAX	%AVG
<b>dummy force</b>	0.00	0.00	0.01	0.00	0.01	0.00	0.00	0.00
<b>inertial</b>	0.03	0.00	1.97	0.07	1.74	0.06	5.87	0.07
<b>pressure</b>	0.00	0.00	-	-	0.00	0.00	0.00	0.00
<b>thermal</b>	0.03	0.00	0.04	0.00	0.04	0.00	3.49	0.08
<b>twist</b>	0.00	0.00	0.00	0.00	0.00	0.00	0.00	0.00

Table 5.1: Second order tetrahedral elements comparison between WB and NS.

### 5.2.2 Inertial Load in PRIME

Simply enough, the inertial load is modeled adding a rotational velocity in the FE model. A boundary condition is required at the shroud in order to simulate the presence of neighboring blades.

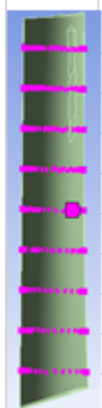
	DISPLACEMENTS						
	SPAN	max difx	avg %errx	max dify	avg %erry	max difz	avg %errz
	10	2.0E-04	0.23	2.5E-03	0.19	4.9E-04	0.09
	9	1.3E-04	0.31	2.2E-03	0.21	3.4E-04	0.10
	8	1.2E-04	0.34	2.0E-03	0.23	3.1E-04	0.10
	7	1.1E-04	0.38	1.8E-03	0.25	2.8E-04	0.11
	6	1.0E-04	0.34	1.6E-03	0.29	2.1E-04	0.10
	5	9.2E-05	0.27	1.3E-03	0.34	1.0E-04	0.07
	4	8.1E-05	0.27	1.0E-03	0.43	1.6E-04	0.15
	3	7.1E-05	0.33	7.2E-04	0.61	2.3E-04	0.49
	2	6.9E-05	0.50	5.8E-04	1.04	2.3E-04	1.34
	1	9.8E-05	0.94	4.2E-04	1.49	3.6E-05	0.58

Table 5.2: Directional displacements results for inertial load




	MAX PRINCIPAL STRESS		
	#	max dif	avg %err
	10	1.4E-02	4.61
	9	6.0E-04	1.11
	8	4.3E-04	0.81
	7	5.0E-04	0.48
	6	5.1E-04	0.37
	5	8.3E-04	0.80
	4	8.9E-04	1.88
	3	9.7E-04	1.45
	2	1.1E-03	1.35
	1	5.7E-03	6.47

Table 5.3: Max principal stress results for inertial load

### 5.2.3 Pressure Load in PRIME

The pressure field acting on the airfoil must be mapped on the 3D mesh, this is done by calculating the average of the source points (pressure map) closest to the target node (FEM mesh). Workbench provides the user with three different mapping algorithms, they use different weightings when computing the average [1]:

- *Triangulation*: a temporary element is created from the three closest source nodes, if the target node is found inside the element, weights are calculated based on the target's location inside the element.
- *Distance Based Average*: it uses the distance from the target node to a specified number of closest source nodes to calculate the weighting value.
- *Kriging*: it is an interpolation algorithm that computes the weighting factors according to their spatial covariance values. It is used for random values maps. Since the pressure acting on the AF is characterized by the presence of gradients and not random values, this method is not further investigated.

In addition pressure can be mapped on corner nodes or on elements, in the first case each node will be associated with a pressure value, while in the second case each element will have a constant pressure value.

In order to choose which method to use, a pressure map has been created and mapped on the face of a plate meshed with tetrahedral elements. Just observing figures 5.7 and 5.8, it is evident that the method that best match the source map is triangulation on corner nodes.

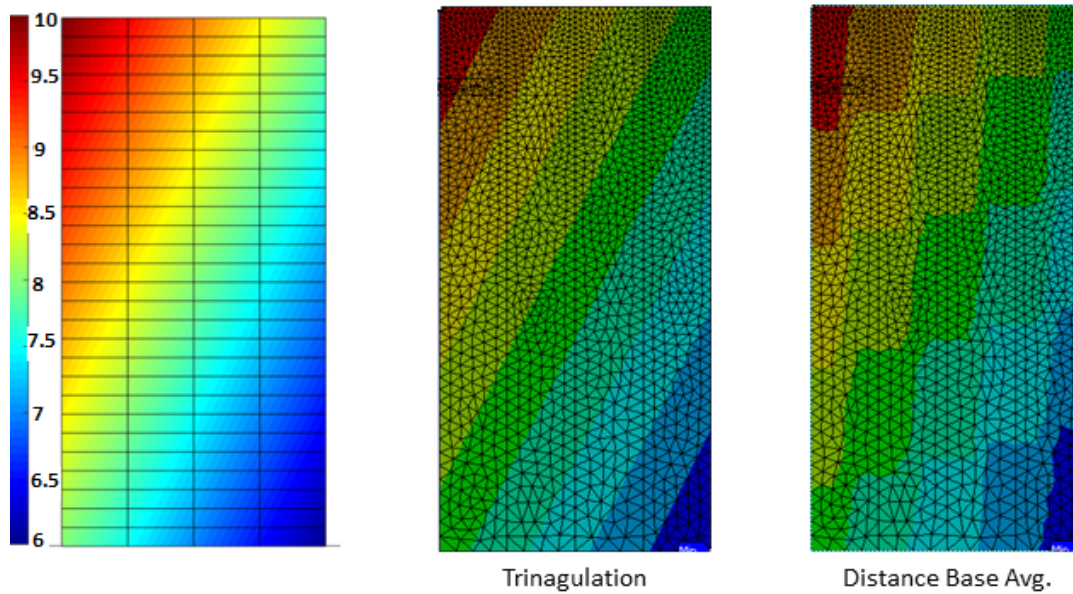


Figure 5.7: Pressure mapping on the nodes of a plate using triangulation and distance based average methods. The plot on the left is the source map.

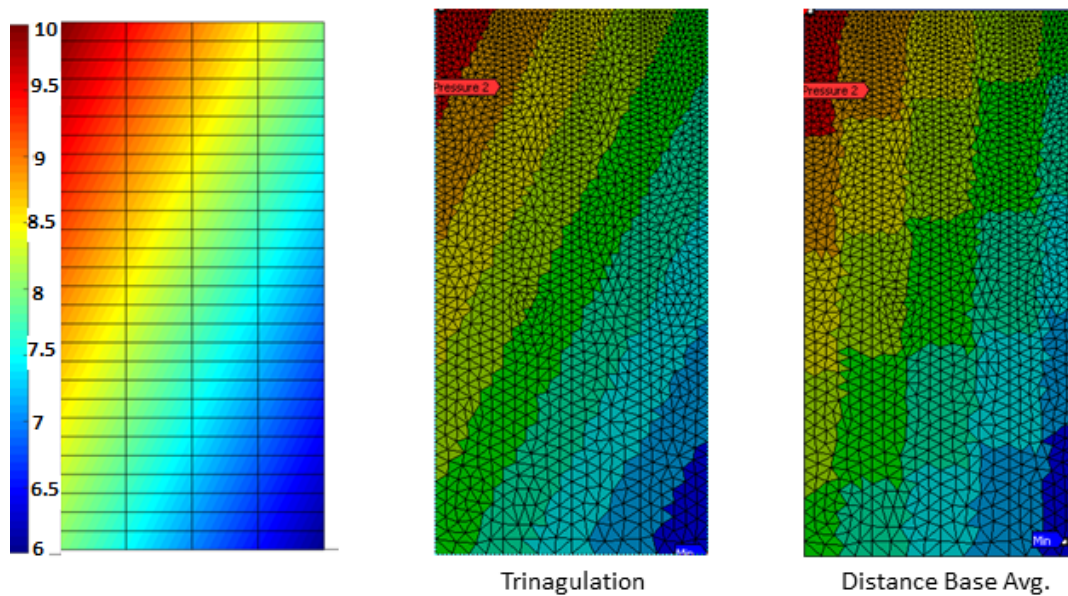


Figure 5.8: Pressure mapping on the elements of a plate using triangulation and distance based average methods. The plot on the left is the source map.

In addition to the pressure load on the airfoil, a boundary condition is required at the shroud as for the inertial case. Below are the tables listing the results.

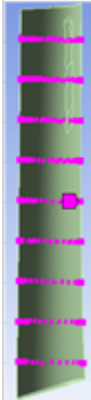
	DISPLACEMENTS						
	SPAN	max difx	avg %errx	max dify	avg %erry	max difz	avg %errz
	10	2.4E-04	0.35	3.8E-03	0.34	1.2E-03	0.47
	9	2.0E-04	0.21	3.1E-03	0.35	1.0E-03	0.53
	8	1.9E-04	0.39	2.7E-03	0.37	1.0E-03	0.59
	7	1.7E-04	0.41	2.5E-03	0.38	1.0E-03	0.64
	6	1.5E-04	0.37	2.2E-03	0.41	9.6E-04	0.70
	5	1.4E-04	0.34	1.8E-03	0.45	8.2E-04	0.77
	4	1.2E-04	0.34	1.4E-03	0.51	6.8E-04	0.90
	3	9.6E-05	0.37	1.1E-03	0.64	5.5E-04	1.17
	2	8.5E-05	0.44	7.7E-04	0.96	4.5E-04	2.04
	1	1.1E-04	0.71	5.0E-04	1.59	3.6E-04	3.19

Table 5.4: Directional displacements results for pressure load


	MAX PRINCIPAL STRESS		
	#	max dif	avg %err
	10	5.9E-03	2.51
	9	2.1E-03	1.79
	8	1.6E-03	0.76
	7	1.6E-03	0.33
	6	1.9E-03	0.30
	5	2.0E-03	0.32
	4	2.2E-03	0.29
	3	2.3E-03	0.25
	2	3.7E-03	0.23
	1	1.3E-02	1.79

Table 5.5: Max principal stress results for pressure load

### 5.2.4 Thermal Load in PRIME

Thermal load is simulated in WB turning on *thermal strain effects*, which allows the use of the *coefficient of thermal expansion*. As in the previous two load cases, a boundary condition is needed at the shroud.

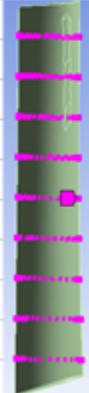
	DISPLACEMENTS						
	SPAN	max difx	avg %errx	max dify	avg %erry	max difz	avg %errz
	10	9.8E-04	0.08	3.6E-03	1.22	7.0E-04	1.82
	9	9.0E-04	0.08	3.2E-03	1.20	5.6E-04	1.72
	8	8.4E-04	0.09	2.9E-03	1.20	5.4E-04	1.90
	7	7.6E-04	0.10	2.5E-03	1.19	4.9E-04	1.06
	6	7.1E-04	0.11	2.2E-03	1.17	4.4E-04	0.74
	5	6.6E-04	0.12	1.8E-03	1.14	3.7E-04	0.54
	4	6.1E-04	0.14	1.4E-03	1.10	2.9E-04	0.39
	3	5.5E-04	0.18	1.1E-03	1.06	2.4E-04	0.27
	2	5.0E-04	0.26	7.0E-04	1.03	2.8E-04	0.18
	1	4.3E-04	0.65	5.0E-04	0.42	3.5E-04	0.15

Table 5.6: Directional displacements results for thermal load


	MAX PRINCIPAL STRESS		
	#	max dif	avg %err
	10	9.5E-04	2.44
	9	9.9E-04	2.42
	8	8.3E-04	4.06
	7	6.1E-04	3.00
	6	2.7E-04	1.41
	5	3.7E-04	1.14
	4	2.4E-04	1.13
	3	4.3E-04	1.87
	2	1.3E-03	2.25
	1	1.8E-02	5.48

Table 5.7: Max principal stress results for thermal load

### 5.2.5 Pre-twist in PRIME

The first step in simulating the pre-twist effects on the structure is the computation of the peanuts plots, from which the interference value between two neighboring blades is derived. In PRIME a simplified version of the peanuts plots is implemented, just two operational conditions are actually simulated, all others are obtained by linear extrapolation. The computation requires the directional displacements of some critical nodes at the tip of the blade, under inertial, thermal and pressure loads. In table 5.8 are listed the WB and NS results on the nodes of interest, normalized to the largest value. It can be noticed that WB and NS give very similar results, the difference being at least one hundred time less than the maximum displacement.

Node	INERTIAL				THERMAL				PRESSURE			
	COND 1		COND 2		COND 1		COND 2		COND 1		COND 2	
	NS	WB	NS	WB	NS	WB	NS	WB	NS	WB	NS	WB
1	0.10	0.10	0.10	0.10	0.95	0.95	0.94	0.94	0.19	0.19	0.19	0.19
2	0.10	0.10	0.10	0.10	0.96	0.96	0.95	0.95	0.20	0.19	0.20	0.20
3	0.25	0.25	0.25	0.25	0.94	0.94	0.93	0.93	0.40	0.40	0.40	0.40
4	0.25	0.25	0.25	0.25	0.96	0.96	0.95	0.95	0.40	0.40	0.40	0.40
5	0.78	0.78	0.78	0.78	0.98	0.98	0.98	0.98	0.79	0.79	0.79	0.79
6	0.79	0.79	0.79	0.78	0.99	0.99	0.99	0.99	0.80	0.79	0.79	0.79
7	1.00	1.00	1.00	1.00	1.00	1.00	1.00	1.00	1.00	1.00	1.00	1.00
8	0.99	0.99	0.99	0.99	0.98	0.98	0.98	0.98	0.99	0.99	0.99	0.99
1	0.97	0.97	0.97	0.97	0.91	0.90	0.92	0.91	0.98	0.97	0.98	0.97
2	1.00	1.00	1.00	1.00	0.92	0.91	0.94	0.93	1.00	1.00	1.00	1.00
3	0.97	0.97	0.97	0.97	0.99	0.98	0.99	0.97	0.96	0.95	0.96	0.95
4	0.99	0.99	0.99	0.99	1.00	0.99	1.00	0.99	0.98	0.97	0.98	0.97
5	0.96	0.96	0.96	0.96	0.46	0.45	0.54	0.53	0.95	0.95	0.95	0.95
6	0.99	0.99	0.99	0.99	0.47	0.46	0.55	0.54	0.97	0.97	0.97	0.97
7	1.00	1.00	1.00	1.00	0.39	0.38	0.49	0.48	0.99	0.99	0.99	0.99
8	0.96	0.96	0.96	0.96	0.38	0.37	0.48	0.47	0.97	0.97	0.97	0.97
1	0.94	0.94	0.94	0.94	0.78	0.77	0.80	0.79	0.87	0.87	0.87	0.87
2	0.96	0.96	0.96	0.96	0.79	0.79	0.81	0.80	0.89	0.89	0.89	0.89
3	0.98	0.98	0.98	0.98	0.99	0.98	0.99	0.98	0.98	0.98	0.98	0.98
4	1.00	1.00	1.00	1.00	1.00	0.99	1.00	0.99	1.00	0.99	1.00	1.00
5	0.69	0.69	0.69	0.69	0.81	0.80	0.79	0.78	0.25	0.25	0.25	0.25
6	0.73	0.73	0.73	0.73	0.82	0.82	0.80	0.79	0.26	0.26	0.26	0.26
7	0.69	0.68	0.69	0.68	0.61	0.61	0.61	0.61	0.15	0.15	0.15	0.15
8	0.65	0.64	0.65	0.64	0.60	0.60	0.60	0.59	0.14	0.14	0.14	0.14

Table 5.8: Peanuts results

Once the peanuts are computed, they can be used to get the moment value to be applied at the blade tip. This load substitutes the boundary condition at the shroud used in the previous cases. In the following table the pre-twist results are listed. For some spans there are no values, because there the results are so small they are cut off by the filter on the order of magnitude.

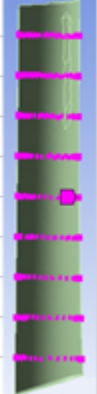
	DISPLACEMENTS						
	SPAN	max difx	avg %errx	max dify	avg %erry	max difz	avg %errz
	10	7.1E-04	1.26	1.7E-02	1.88	1.6E-02	1.43
	9	2.9E-04	0.74	1.2E-02	1.38	1.1E-02	1.24
	8	2.3E-04	0.64	8.3E-03	1.34	7.2E-03	1.16
	7	1.9E-04	0.70	5.8E-03	1.30	4.8E-03	1.12
	6	1.3E-04	0.68	4.0E-03	1.24	3.1E-03	1.09
	5	-	-	2.5E-03	1.27	1.8E-03	1.10
	4	-	-	1.6E-03	1.26	1.0E-03	1.12
	3	-	-	9.2E-04	1.33	5.4E-04	1.24
	2	-	-	4.9E-04	1.68	2.8E-04	1.63
	1	-	-	-	-	-	-

Table 5.9: Directional displacements results for pre-twist


	MAX PRINCIPAL STRESS		
	#	max dif	avg %err
	10	6.2E-02	9.74
	9	1.8E-02	2.78
	8	1.7E-02	2.99
	7	1.6E-02	3.16
	6	1.3E-02	3.07
	5	1.1E-02	3.01
	4	8.1E-03	2.54
	3	6.1E-03	2.23
	2	4.4E-03	1.97
	1	3.3E-03	3.85

Table 5.10: Max principal stress results for pre-twist



### 5.2.6 Complete Load Case

Since the static analysis conducted in PRIME is linear, the superimposition of effects principle is valid and the results of the single load cases can be summed together, in order to obtain the complete case.


	DISPLACEMENTS						
	SPAN	max difx	avg %errx	max dify	avg %erry	max difz	avg %errz
	10	7.9E-04	0.07	3.7E-03	0.37	6.4E-04	0.10
	9	6.6E-04	0.08	3.1E-03	0.40	2.8E-04	0.05
	8	6.1E-04	0.09	2.8E-03	0.42	1.2E-04	0.03
	7	5.6E-04	0.10	2.6E-03	0.46	1.6E-04	0.09
	6	5.2E-04	0.11	2.3E-03	0.51	1.6E-04	0.13
	5	4.8E-04	0.12	1.9E-03	0.57	9.3E-05	0.10
	4	4.4E-04	0.15	1.5E-03	0.66	1.5E-04	0.33
	3	4.0E-04	0.19	1.1E-03	0.78	2.2E-04	0.36
	2	3.6E-04	0.28	8.2E-04	0.98	2.9E-04	0.28
	1	3.3E-04	0.70	5.9E-04	0.75	3.1E-04	0.15

Table 5.11: Directional displacements results for the complete case


	MAX PRINCIPAL STRESS		
	#	max dif	avg %err
	10	1.0E-02	3.12
	9	2.9E-03	4.35
	8	3.0E-03	3.27
	7	2.9E-03	2.57
	6	2.8E-03	1.95
	5	2.6E-03	1.64
	4	1.9E-03	1.05
	3	1.5E-03	0.79
	2	1.2E-03	0.55
	1	1.1E-02	3.33

Table 5.12: Max principal stress results for the complete case

The results obtained are consistent with the expectations derived from the elements investigation. The displacement average error along the span is always below 2% in all load cases. It has very small values in the central spans and it grows while

approaching the fillets. This is due to the higher geometry complexity in these regions, where the mesh struggle to follow the curvature of the body. The same trend can be seen on the maximum principal stress results, but the errors are larger, due to the additional computation the software has to make in order to retrieve these results. Another source of error is the way pre-twist is applied. Since the method used in design practice can't be easily transferred to PRIME, a simplified approach is used, which consists in the application of a moment at the blade tip. Nevertheless the interference load has minor effects on the complete case, making this method acceptable. In conclusion, the overall case well approximates the Nastran displacement solution (average error lower than 1%). When it comes to stress results, some larger errors occur in those areas affected by fillets and pre-twist.



# Chapter 6

## Forced Response

High Cycle Fatigue (HCF) is one of the main failure mechanisms in turbomachinery components, especially flow-path components like turbine blades. It manifests itself through increased engine development time and costs and increased maintenance efforts. In new engine designs, the issue becomes even more complex. Because of the augmented demand for higher thrust-to-weight ratios and reduced fuel consumption, higher pressure ratio turbine stages are required and new stage configurations are studied, as the integrally bladed disk or blisk (i.e. blade and disk consist of a single part). These requirements result in highly stressed blades with high modal densities and increased aerodynamic excitation, all precursory indicators of potential HCF issues.

While Low Cycle fatigue failure mode has a relatively long propagation-to-failure life after crack detection, in HCF the crack takes a longer time before it reaches a detectable size, but the propagation-to-failure life is very short. Moreover bladed disks are subjected to large driving frequencies. These two aspects combined may lead to failure in minutes, making HCF extremely dangerous. Thus it is evident why resonant frequencies must be studied in details.

As already mentioned in chapter 2.2.2, the Campbell diagram is a powerful instrument to detect potential resonance conditions. Nevertheless crossings in the operative range of the engine may be unavoidable. These conditions are usually higher-order modes with presumed weaker drivers that can be further analyzed [5]. The focus of this chapter is the detailed analysis of crossing conditions, in order to understand if they represent a danger or can be tolerated by the structure. The activity conducted with Avio Aero is the automation of an already existing tool (@Forced) property of the company, in order to fit it in the PRIME process.

The tool @Forced computes the work done by the aerodynamic excitation on a specific mode. Besides a global index is calculated, the *Modal force*. It is a measure

of the extent of resonance phenomena, the larger the value the more the structure is excited by the aerodynamic force.

## 6.1 @Forced for PRIME

The tool @Forced works through a GUI (figure 6.1). The user has to manually insert a number of inputs, which can be divided in two groups:

- FEM data: they consist of FEM mesh, modeshapes, engine axial axis and number of airfoils analyzed.
- CFD data: the unsteady pressure field around the blade profile.

Afterwards the actual computation of the aerodynamic work on the mode is carried out and the modal force is displayed. The post processing includes a number of plots, through which the user can monitor the tool process. For instance he can check if the pressure has been properly mapped from the CFD grid to the FEM mesh, or he can verify if the imported modashape and pressure fields are the correct ones.

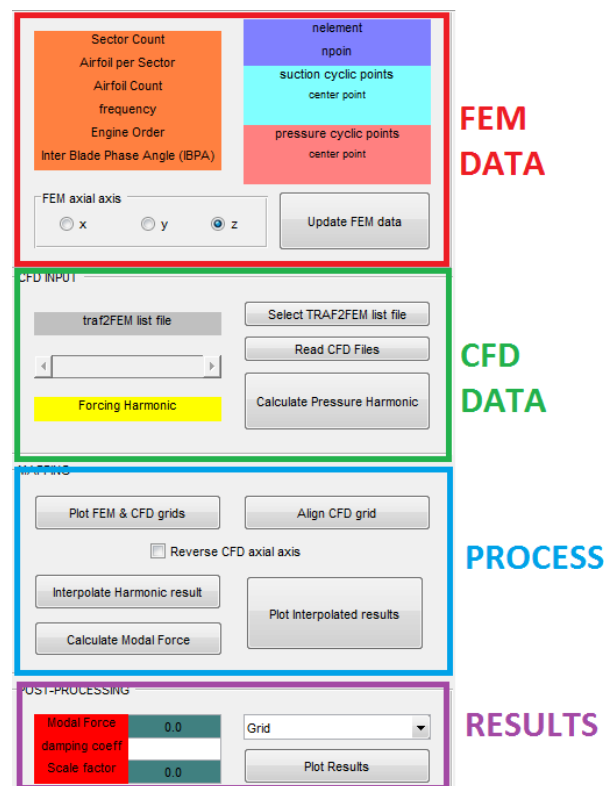


Figure 6.1: @Forced GUI

In order to fit @Forced in PRIME, the tool must be automatized and the GUI eliminated. Since PRIME is based on a standard process, it is relatively easy to develop a routine which automatically imports all necessary data, runs the computation and stores the outputs. In the specific case, FEM data are generated by a modal analysis previously performed by a WB Wizard. Since the model is standard, the engine axis is always the same and a single airfoil is analyzed. CFD data are provided by the user and processed through FTL, in order to have the needed maps. Once all information are imported, the process can start. For a good mapping of the pressure on the FEM mesh, a good overlap of the CFD and FEM grids must be achieved. While an automatic evaluation of the needed axial translation and stretch of the CFD grid was already present, the radial movement and stretch have been introduced in the PRIME version of the tool. Eventually all output plots and data are stored in a specific area of the folder tree created by PRIME.

## 6.2 Tool Process

The process of the @Forced routine developed for PRIME is displayed in figure 6.2. Inputs and outputs are in orange, while the functional blocks are in blue.

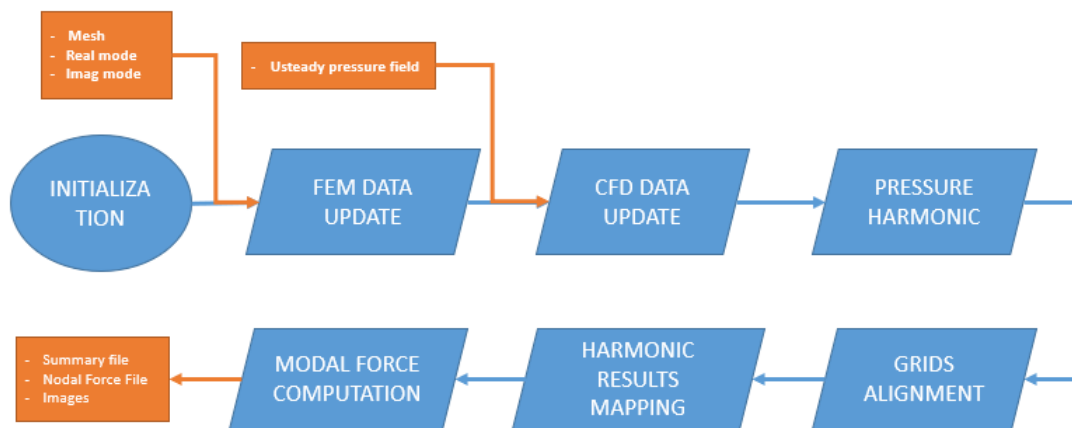


Figure 6.2: @Forced process

After all necessary data are read and properly stored, the routine computes the pressure harmonic. Pressure information are organized such that the time evolution of the unsteady field is available for further elaboration. A Fast Fourier Transform is applied in order to obtain the mean pressure value over the analyzed time period.

and the magnitude and phase of the pressure harmonic. This way, using just three CFD maps, the behavior of the unsteady flow is caught.

Since CFD and FEM data comes from two different sources, there may be a misalignment of the grids. It is important to align them before mapping pressure data on the FEM mesh. The amount of radial and axial relocation is computed taking into account the locations of two points: one in the middle of the trailing edge, the other in the middle of the hub line (figure 6.3). In addition the CFD grid is stretched to obtain a full cover of the airfoil.

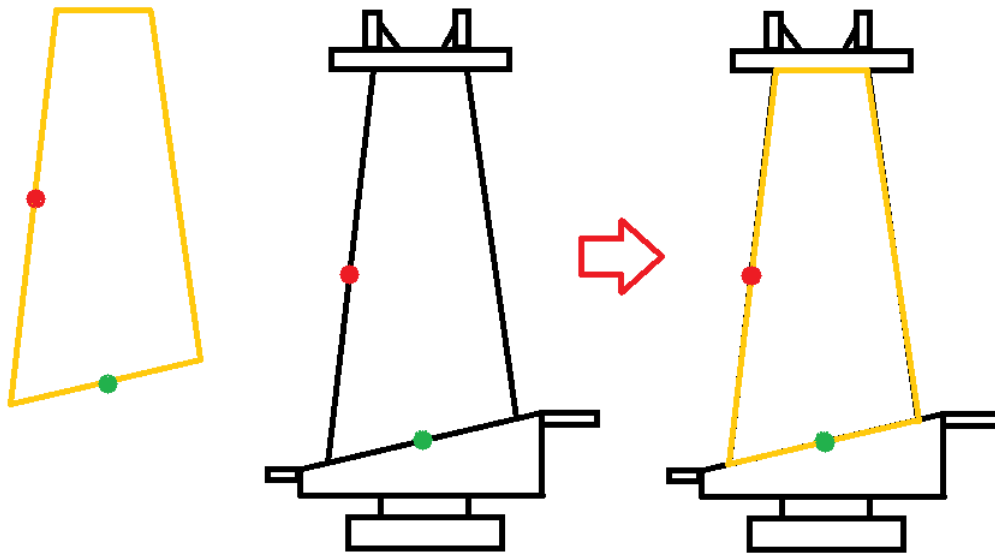


Figure 6.3: Grid alignment. The red point is used for axial alignment, while the green point for radial alignment

Once the maps are aligned, the exciting action can be transferred on the FEM mesh. The work is computed by multiplying the modal displacements by the aerodynamic force acting on each element. Furthermore a *Frequency Response Function* (FRF) is used to derive two indexes which describe the global behavior of the blade: the modal force and the scale factor. In figure 6.4 the plot of the scale factor over the ratio between exciting and natural frequencies is displayed, the peak indicating resonance condition is approached when  $\omega = \omega_n$ . If the peak value is large, it means the resonance phenomenon acting on the structure is dangerous. In this case the blade must be redesigned in order to achieve a larger damping of the oscillations. In the redesigning process engineers may need information about where on the airfoil

the exciting action has the greatest effect, this local information is provided by plotting the work acting on each element of the FEM mesh. Eventually a file is printed, containing equivalent forces on every nodes so that their work will lead to the same resonance condition obtained with the pressure exciting action.

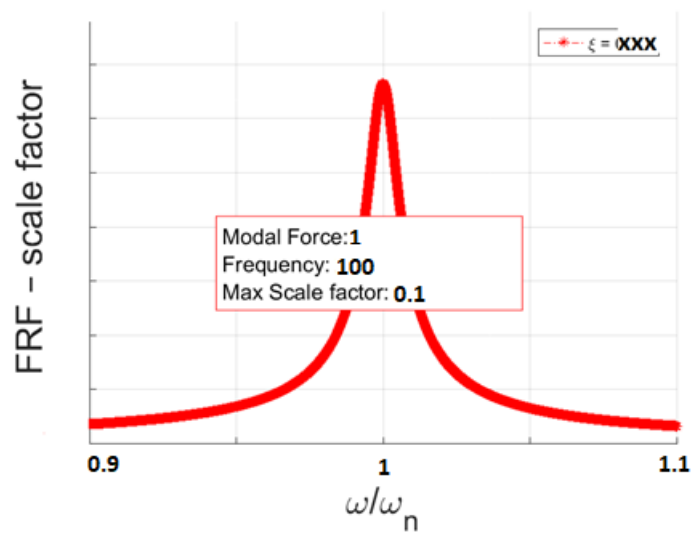


Figure 6.4: FRF: frequency response function



# Chapter 7

## Conclusions

The long term goal of this thesis work is to rethink the way preliminary design is performed, defining a new procedure that will include in the optimization loop both aerodynamic and structural mechanic disciplines. In order to make the Aero-Mech design possible, a tool (PRIME) able to give quick mechanical feedback is needed. This thesis places itself in this context, more specifically a new simulation method for static structural analysis to be performed in Ansys Workbench has been developed, and an already existing routine for forced response analysis has been automatized.

When it comes to static analysis, the results obtained with the newly developed simulation procedure have been compared to those obtained following the design practice of the company, which makes use of the software msc Nastran. The results have been found to be close enough for a preliminary assessment of the mechanical behavior of the structure. The new static structural project has been implemented inside a wizard in the Ansys Workbench environment, able to set and solve the FEM model automatically.

As far as the forced response is concerned, the automation of the @Forced tool made possible to fit it inside the PRIME process. It takes as inputs structural information from the wizard and aerodynamic data from a routine which processes inputs provided by the user.

In conclusion the PRIME process provides a fast, easy and automatic way to perform a preliminary assessment of the mechanical response of LPT stages, allowing its integration in the aerodynamic optimization loop. The optimum point computed using the Aero-Mech process is the best compromise between performance and mechanical response, leading to the reduction of fixings in the detailed design phase.





# Appendix A

## PRIME Routines Overview

The PRIME tool is made of many routines, which implement different functionalities of the process. This appendix is an overview of all these routines, their purpose is delineated and a general description of their working mechanism is given.

### A.1 DynBooster

The bottleneck between aerodynamic and structural design is the definition of the CAD model. CFD analyses are used to define the shape of the airfoil, exclusively studying its interactions with the airflow. Instead, to perform a structural analysis, the geometry must be completed with the elements at the ends of the AF, in order to simulate the contacts. This operation can be very time consuming. The tool *DynBooster* has the goal to take all the needed actions to create the complete CAD automatically. Because time is an important parameter when it comes to preliminary design, the routine uses a parametric approach to define the geometries to be attached to the airfoil. Thus the user is given a simple and fast way to modify the shape of the elements.

The first step in the DynBooster process is the creation of the 3D airfoil. The tool reads the aerodynamic data, from which it extrapolates all the information about the 2D hub and tip airfoils. Through the use of auxiliary splines the 2D airfoils are stacked up and the tri-dimensional geometry is built. Aerodynamic data are not just useful for the generation of the blade profile, but some information are needed when attaching the required elements to the AF as well. Hence the data are stored in an easy-to-access file with a standard layout.

As already mentioned DynBooster uses parametric templates to define the elements to be attached to the airfoil. Each template is characterized by two sets of parameters:

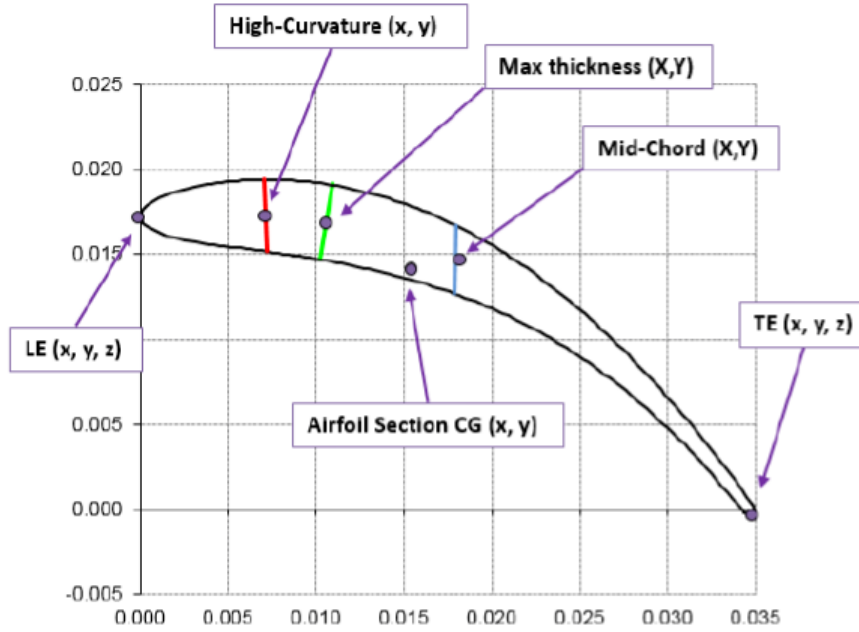


Figure A.1: 2D airfoil and the parameters that define it [12]

- The *System Parameters* are automatically updated by the tool, the user can't change them. They are computed from some information about the 2D cross sections at the tip and hub of the airfoil, namely:
  - The incline of the AF at the ends of the blade;
  - The chord length;
  - The spatial coordinates of leading and trailing edge;
  - The radial distance of the ends from the engine axis.
- The *Custom Parameters* can be modified by the user, who uses them to change shape and dimension of the templates to best fit his needs. They are grouped into: lengths, thicknesses, radii, fillets and angles.

All the parameters are conveniently scaled with respect to the AF dimension before the user can modify them, so that a single template can be used for all the engine stages. The templates must comply with two fundamental requirements: they must be representative of a real geometry and their parameterization must be easy and robust. In order to fulfill these conditions they have been created starting from a cross section of an existing engine, from which a 2D sketch has been derived. The 3D geometry is produced by revolving the sketch around the engine axis, then the shape is refined with trimming operations.

The user can either choose to generate a standard CAD, i.e. OBV and IBV will be added to the vane, fixing, shank and shroud to the blade, or he can create a custom CAD, choosing an unusual configuration of templates. In figure A.2 the GUI through which the user can make this choice is displayed, all the available templates are shown too.

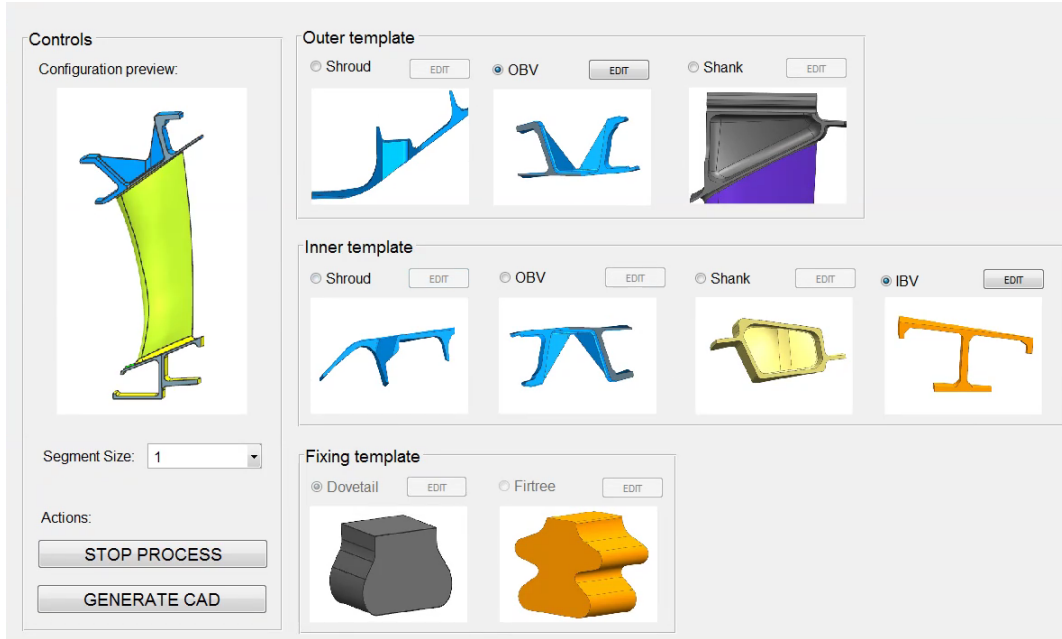


Figure A.2: DynBooster GUI for templates selection

The templates positioning with respect to the airfoil is a crucial point in the DynBooster process. Each geometry is imported near the center of gravity of the end to which it must be attached. Then it is moved through the definition of an axial and tangential offset, until the desired position is reached. The offsets are computed using the aerodynamic data previously mentioned and are defined with respect to four points on the AF:

- Leading edge
- Trailing edge
- Maximum thickness point
- Maximum curvature point

Eventually the fillets are created in order to generate a single body. The last step is to tag some surfaces which will later be used for applying boundary conditions, loads or for mesh refinement.

## A.2 Wizard

Ansys Workbench is used to perform FE analyses. The process is automatized through the programming of a *wizard*, which allows the creation of a GUI, through which the user can run a determinate sequence of actions automatically carried out by WB. Up to the moment this thesis is written, the wizard is able to perform different analyses on a vane model or a blade only model. In table A.1 the available analyses for each model are listed.

Vane Model	Blade Only Model
Modal analysis	Pre-stressed modal analysis
	Peanuts plots computation
	Static analysis

Table A.1: Analyses available in the WB wizard

The starting point of the wizard is the CAD generated by DynBooster. The only requirement on the CAD is the presence of specific *Named Selections* (i.e. tagged geometry features, usually surfaces), which will be used to refine the mesh in certain areas or to apply load and boundary conditions or for solution post-processing.

After the CAD has been imported, the Wizard generates the mesh. Particular attention is put at the airfoil fillets and at the leading and trailing edge, since in these regions smaller elements are required because of the curvature of the geometry. A different *Static Structural* block is created for each analysis, here the boundary conditions and the loads are applied. Pressure and temperature fields are provided by the user, as well as the rotational velocity value. A library of commonly used material is available inside the WB project, from which the user can choose freely. The Wizard has the capability to deal with more than one operative conditions, in this case each condition is run at a different time step inside the static structural block, while multiple modal blocks are used for the modal analysis. As it can be seen from figure A.4, a specific analysis requested by the user may need more than one block, for instance the peanuts plots computation requires 4 separate static analyses: one for the stiffness computation and 3 for the loads applied separately.

The Wizard generates many outputs depending on the type of analysis launched, which are organized inside a folders tree:

- Peanuts plots

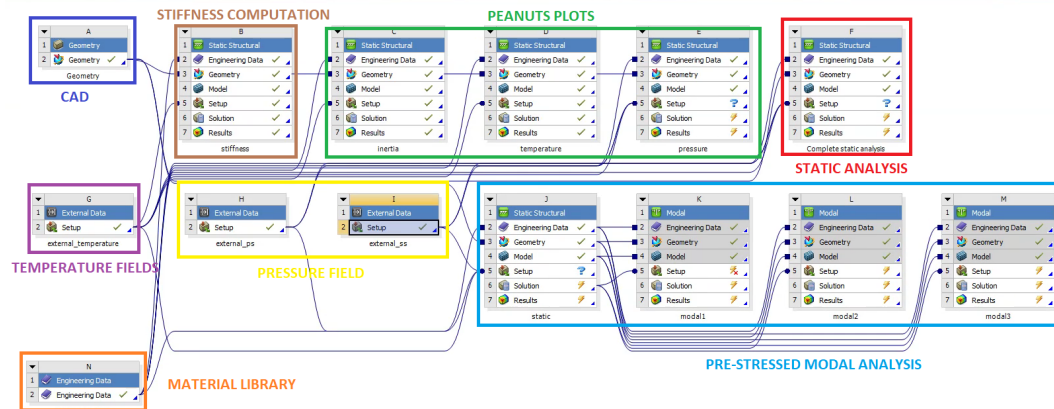


Figure A.3: WB project automatically generated by the Wizard for a blade only model. In this case all the analyses have been requested (peanuts plots computation, static analysis and modal analysis)

- Static analysis: all the outputs produced by this analysis, together with the peanuts plots, are collected inside a dashboard. Here the stresses along the airfoil span are plotted both for pressure and suction side, a good airfoil won't have a too large difference between the two sides. The displacements are checked on specific points, in order to guarantee clearance around the body. Eventually color maps for stresses are provided for different regions of the blade, namely: fixing, shank, hub and tip fillets, airfoil and shroud.
- Modal analysis: from this study all the modeshapes and corresponding frequencies are derived, afterward the Campbell diagram is drawn. The reports for flutter analysis and forced response are generated too.

All the actions undertaken by the Wizard are "invisible" to the user, who just needs to provide some inputs through a GUI:

- 1- CAD import.
- 2- Model type: vane or blade only.
- 3- Material choice.
- 4- Analysis types.
- 5- Operating conditions: rotational velocity, pressure and temperature fields. Not all these inputs are required, depending on the model and the analysis types selected.
- 6- Outputs request.

### A.3 @Forced

The software @Forced is used to study the forced response of the structure. When a crossing on the Campbell diagram occurs in the operative range of the engine, the forced response in that condition must be analyzed, in order to verify to which extent resonance takes place. This analysis is especially needed in those cases in which the resonance condition on the Campbell diagram cannot be easily removed. The goal is to check if the exciting action on a specific mode, due to the unsteady flow around the blade, can be tolerated by the structure.

The necessary inputs are the modeshape, both real and imaginary part are needed in case of a rotating mode, and the time evolution of the pressure field around the airfoil. The steps executed by @Forced are listed below:

- 1- FEM files import: modal displacements and mesh information.
- 2- CFD files import: pressure maps.
- 3- Pressure harmonic computation: three maps are created, one containing the mean value of the pressure at each point of the CFD grid, the other two including the magnitude and phase of the principal harmonic of the unsteady pressure field.
- 4- CFD and FEM grids alignment.
- 5- Data transfer from CFD grid to FEM mesh.
- 6- Modal force computation.

The main output of this routine is the *Modal force*, a measure of the work done by the aerodynamic action on the mode, and a nodal force file, which contains a complex force value for each node of the FEM mesh, this exciting action has the same effect on the mode as the unsteady pressure field. The modal force allows for a quick assessment of the resonance magnitude, a too large value means that the blade won't tolerate the analyzed condition.

### A.4 AutoFlutter

FTL studies the interactions between fluid and structure, in order to foresee if flutter phenomena will arise. Flutter is an auto-excited vibration of the structure. In certain

conditions the aerodynamic forces are able to modify the free oscillation characteristics of the system. The extent to which the free response is altered depends mainly on the ratio between fluid and structure mass. In the case of turbine blades, flutter phenomena usually arise for a single mode at frequencies near its natural frequency. If the system is not damped enough, the magnitude of the oscillations rises until the structure breaks. Once the flutter is triggered, it develops very quickly making these phenomena extremely dangerous. This is due to the large amount of kinetic energy in the flow, much larger than the energy that the structure can possibly absorb[7].

The aerodynamic exciting force acts on random directions and is generally out of phase with respect to the mode of vibration. The ability of the system not to incur in flutter phenomena is mainly due to aerodynamic damping, due to the out-of-phase component of the exciting action. The aerodamping is ultimately a measure of the amount of energy absorbed by the structure. Negative values mean unstable vibrations arise.

FTL has the goal to compute the aerodamping. It makes use of both aerodynamic data, derived from CFD analyses performed on the blade profile, and FEM data, i.e. the modeshapes for each nodal diameter of a specific vibration mode. The software produces a plot of the aerodynamic damping coefficient for all the IBPA values.

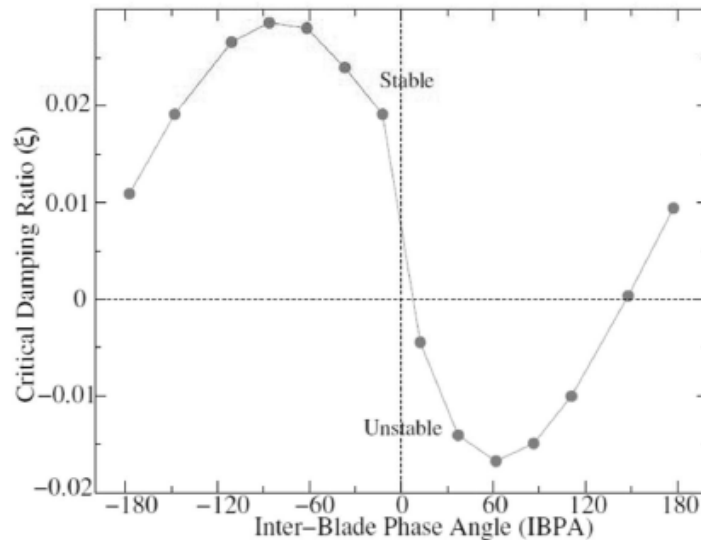


Figure A.4: Aeroplots example [7]





# Bibliography

- [1] ANSYS. Workbench user's guide. *ANSYS Inc., Canonsburg, PA*, 2018.
- [2] G Battiato, CM Firrone, TM Berruti, and BI Epureanu. Reduced order modeling for multi-stage coupling of cyclic symmetric structures. In *International Conference on Noise and Vibration Engineering and International Conference on Uncertainty in Structural Dynamics (ISMA/USD), Leuven, Belgium, Sept*, pages 19–21, 2016.
- [3] Giuseppe Battiato. Progetto di un simulacro di turbina per uso aeronautico per test dinamici con tecnica di misura blade tip timing. master thesis, Politecnico di Torino, 2013.
- [4] Giuseppe Battiato. Vibrations prediction and measurement of multi-stage bladed disks with non linear behavior due to friction contacts. phd thesis, Politecnico di Torino, 2017.
- [5] Joseph A Beck. Fundamental understanding of blisk analytical response. 2013.
- [6] Fabio Bellacicco. Stabilizzazione di uno stadio di lpt bladed-disk in presenza della condizione di instabilità a flutter mediante mistuning intenzionale. master thesis, Politecnico di Torino, 2016.
- [7] Andrea Bray. Interazione fluido-struttura in turbine aeronautiche di bassa pressione. master thesis, Politecnico di Torino, 2018.
- [8] L. Casalino and D. Pastrone. Fondamenti di macchine. Appunti accademici, Politecnico di Torino, 2014.
- [9] Matthew P Castanier, Yung-Chang Tan, and Christophe Pierre. Characteristic constraint modes for component mode synthesis. *AIAA journal*, 39(6):1182–1187, 2001.

- [10] Luca Cipressa. Study of new simulation method for lp turbine row, trade-off study and assessment. master thesis, Politecnico di Torino, 2017.
- [11] Kiran X D’Souza and Bogdan I Epureanu. A statistical characterization of the effects of mistuning in multistage bladed disks. *Journal of Engineering for Gas Turbines and Power*, 134(1):012503, 2012.
- [12] Andrea Ferrante. Sviluppo di un tool per studio dinamico automatizzato relativo a palette di turbine di bassa pressione. master thesis, Politecnico di Torino, 2018.
- [13] P. G. Hill and C. R. Peterson. *Mechanics and Thermodynamics of Propulsion*. Addison-Wesley, Reading, Massachusetts, second edition, 1992.
- [14] Jianfu Hou and Bryon J. Wicks. Root flexibility and untwist effects on vibration characteristics of a gas turbine blade. *Defence science & technology*, 2002.
- [15] J. F. Louis. Axial flow contra-rotating turbines. *ASME*, 85-GT-218, 1985.
- [16] L. Moroz, P. Pagur, Y. Govoryshchenko, and K. Grebennik. Comparison of counter-rotating and traditional axial aircraft low-pressure turbines integral and detailed performances. *ICHMT*, 2009.
- [17] Regione Piemonte. Great 2020, 2012. <http://www.great2020.it/index.html>.
- [18] Kalapala Prasad, B Anjaneya Prasad, and M Anandarao. Optimization of twisted aero-foil blade angle of a structural gas turbine assembly. *International Journal of Applied Engineering Research*, 12(15):4818–4824, 2017.
- [19] Rolls-Royce. *The Jet Engine*. Rolls-Royce plc, Derby, England, fifth edition, 1996.
- [20] Brian J Schwarz and Mark H Richardson. Experimental modal analysis. *CSI Reliability week*, 35(1):1–12, 1999.
- [21] Murari P. Singh, John J. Vargo, Donald M. Schiffer, and James D. Dello. Safe diagram - a design and reliability tool for turbine blading. *Proceedings of the seventeenth turbomachinery symposium*, 1988.
- [22] Garry J Tee. Eigenvectors of block circulant and alternating circulant matrices. 2005.

- 
- [23] D. L. Thomas. Dynamics of rotationally periodic structures. *International Journal for Numerical Methods in Engineering*, 1979.
  - [24] Paolo Turrone. Studio della dinamica di settori palettati statorici nelle turbomacchine per impiego aeronautico. master thesis, Politecnico di Torino, 2015.
  - [25] David P. Walls, Robert E. deLanueville, and Susan E. Cunningham. Damage tolerance based life prediction in gas turbine engine blades under vibratory high cycle fatigue. *ASME*, 1995.